

25X1

EVALUATION OF COHERENT ENLARGER (U)

FINAL REPORT

**Declass Review by NIMA / DoD**

**CONFIDENTIAL**

25X1

EVALUATION OF COHERENT ENLARGER (U)  
FINAL REPORT

25X1

July, 1966

This document contains information affecting the national defense of The United States within the meaning of the Espionage Laws, Title 18, U.S.C., sections 793 and 794. Its transmission or the revelation of its contents in any manner to an unauthorized person is prohibited by law.

25X1

**CONFIDENTIAL**

25X1

Approved For Release 2002/07/12 : CIA-RDP78B04747A002700020022-7

Approved For Release 2002/07/12 : CIA-RDP78B04747A002700020022-7

## A B S T R A C T

The imaging properties of a coherent enlarger were evaluated theoretically and experimentally. Images of partially coherent objects were analyzed, and both the coherence of the object plane illumination and the incoherent transfer function of the optical system were measured directly. The theory of partial coherence was used to predict the image intensity distribution for certain test objects illuminated by partially coherent light; experiments confirmed the predictions. Spatial filtering applications were considered. The instrument was found to have useful applications as an enlarger and a spatial filtering system.

25X1

Approved For Release 2002/07/12 : CIA-RDP78B04747A002700020022-7

25X1

Approved For Release 2002/07/12 : CIA-RDP78B04747A002700020022-7

## TABLE OF CONTENTS

<u>Chapter</u>		<u>Page</u>
1	INTRODUCTION AND SUMMARY . . . . .	1
2	THEORY OF PARTIALLY COHERENT IMAGING . . . . .	4
	BASIC DEFINITIONS . . . . .	4
	MUTUAL COHERENCE FUNCTION . . . . .	4
	COHERENT AND INCOHERENT FIELDS . . . . .	6
	THE VAN CITTERT-ZERNIKE THEOREM . . . . .	7
	THE IMAGING PROBLEM . . . . .	7
	EXAMPLES OF PARTIALLY COHERENT IMAGING . . . . .	11
	Cosine Targets . . . . .	11
	Edge Objects . . . . .	18
3	DEGREE OF COHERENCE IN THE OBJECT PLANE . . . . .	24
	THEORETICAL PREDICTION . . . . .	24
	EXPERIMENTAL MEASUREMENTS . . . . .	32
4	INCOHERENT TRANSFER FUNCTION MEASUREMENTS . . . . .	37
5	IMAGING STUDIES . . . . .	43
	THEORETICAL AND EXPERIMENTAL . . . . .	44
	EDGE IMAGES . . . . .	44
	" L " TARGETS . . . . .	49
	EXPERIMENTAL . . . . .	55
	USAF THREE-BAR TARGETS . . . . .	55
	SQUARE-WAVE TARGET . . . . .	55
6	SPECIAL CASES IN WHICH PARTIALLY COHERENT SYSTEM BECOMES LINEAR IN INTENSITY . . . . .	59
	LOW-CONTRAST OBJECTS . . . . .	59
	OBJECTS WITH LOW SPATIAL-FREQUENCY CONTENT . . . . .	66

## TABLE OF CONTENTS (Cont'd.)

<u>Chapter</u>		<u>Page</u>
7	PARTICULAR COHERENCE EFFECTS . . . . .	70
	COHERENCE NOISE . . . . .	70
	EXAMPLE OF NONLINEAR EFFECTS . . . . .	72
8	SPATIAL FILTERING APPLICATIONS . . . . .	75
	RASTER REMOVAL . . . . .	75
	FILTERS SUPPLIED WITH ENLARGER . . . . .	78
9	CONCLUSIONS AND RECOMMENDATIONS . . . . .	81
	REFERENCES . . . . .	83
APPENDIX A.	AERIAL SCENES . . . . .	A-1
APPENDIX B.	COMPUTER PROGRAM FOR FINDING THE INTENSITY IN THE IMAGE OF A PARTIALLY COHERENT OBJECT . . . . .	B-1
APPENDIX C.	RASTER REMOVAL . . . . .	C-1


## LIST OF ILLUSTRATIONS

<u>Figure</u>		
1	Simplified Optical Schematic of Enlarger . . . . .	7
2	Direct Imaging of Cosine Targets . . . . .	11
3	Apparent Transfer Function Measured for Fundamental Term of Sine Wave Targets . . . . .	17
4	Apparent Transfer Function for Second Harmonic Term . . . . .	17
5	Apparent Transfer Function from an Edge Trace . . . . .	23
6	Intensity Across Single Mode Laser Beam vs Gaussian of Halfwidth 0.8 mm . . . . .	24
7	Experimental Arrangement for Measuring Degree of Coherence . . . . .	32



## CHAPTER 1

## INTRODUCTION AND SUMMARY

The imaging properties of the  photographic enlarger shown in Figure 1 were evaluated. The distinctive feature of this enlarger is its use of partially coherent light to illuminate the object transparency. The principal part of this program was therefore to determine the effects of this mode of illumination on the relation between object and image. Other important areas of investigation were to assess the optical quality of the system and its use as a spatial filtering system.

25X1

The theory of partial coherence outlined in Chapter 2 was applied to the present imaging situation. For partially coherent illumination, the customary image evaluation criteria and techniques for determining the relation between object and image do not apply since the imaging system is not linear in intensity. Generally, the intensity distribution in the image is determined by (1) the coherence of the illumination over the object plane, (2) the amplitude impulse response of the optical system, and (3) the amplitude transmittance of the object transparency. To find the relation between object and image, all three must therefore be determined.

The degree of coherence in the object plane was measured directly, using a two-pinhole interferometer. The results are reported in Chapter 3. For the case of the rotating ground glass illuminated by the laser (single mode or multimode), we found that the ground glass is an effectively incoherent source. The degree of coherence measured in the object plane proved to be the same as that predicted by applying the well known van Cittert-Zernike theorem to this incoherent source. An independent theoretical prediction of the ensemble-averaged degree of coherence in the radiation from a rough glass surface provided further confirmation of these results.

We found that on-axis the experimentally measured incoherent transfer function of the enlarger is very close to that which would be obtained from a diffraction-limited system. (Measurements of on-axis resolution are given in Chapter 4; those for off-axis in Chapter 5.) For theoretical work in the remainder of the program, the amplitude impulse response on-axis was therefore taken to be that of a diffraction-limited system.

25X1



25X1

Approved For Release 2002/07/12 : CIA-RDP78B04747A002700020022-7

25X1

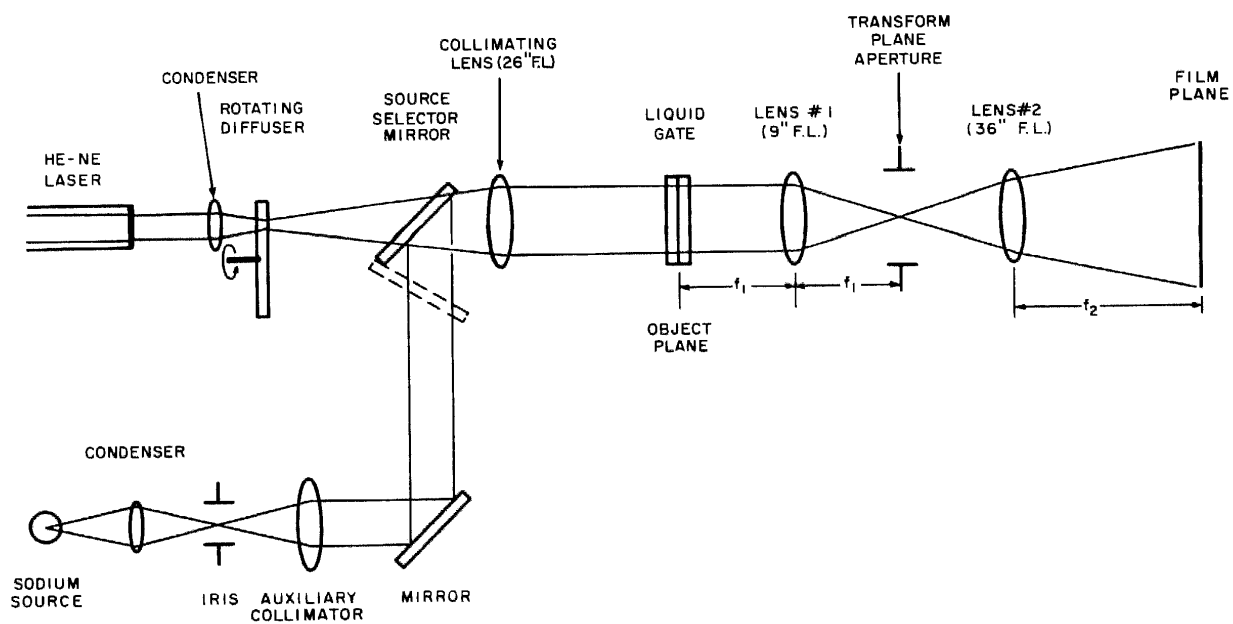


Figure 1. Simplified Optical Schematic of Enlarger

Approved For Release 2002/07/12 : CIA-RDP78B04747A002700020022-7



To illustrate some of the unusual effects that occur in imaging with partially coherent illumination, the experimentally determined images of edge objects and some commonly used resolution targets are presented in Chapter 5. Using the results of Chapters 3 and 4 and the known amplitude transmittance of these objects, we were able to determine the images of several of them theoretically. The computer program used for these calculations is given in Appendix B. The theoretical and experimental images are in excellent qualitative, and in fairly good quantitative, agreement. Some typical aerial scenes were also imaged under several conditions of coherence and these are included in Appendix A.

There are two special cases in which an optical system becomes linear in intensity even though the illumination of the object transparency is partially coherent. These are analyzed in Chapter 6. Although a transfer function can be defined for such systems, coherence effects remain, since the form of the transfer function depends on the degree of coherence of the illumination. The applicability of these two limiting cases to practical enlarging applications is discussed.

Two of the prominent effects of partially coherent illumination are treated in Chapter 7.

A promising application of the enlarger is treated in Chapter 8. The coherence of its illumination permits spatial filtering, and this technique has been used to remove raster from certain photographic scenes. The results are of good quality because of the quality of the enlarger optics and possibility of varying the degree of coherence in the object plane.

The conclusions arrived at in this program and technical recommendations for further use of the enlarger comprise Chapter 9.

## CHAPTER 2

## THEORY OF PARTIALLY COHERENT IMAGING

The structure for a fundamental treatment of image formation problems already exists in the formalism of modern coherence theory as introduced by Wolf.<sup>1</sup> An adequate introduction to the subject is provided by Born and Wolf (Ref. 2, Chap. 10), and a detailed description of some of the results of the theory to date may be found in Beran and Parrent.<sup>3</sup> Therefore it will not be necessary to review the subject extensively here. Rather, we shall limit ourselves to a statement of the pertinent definitions and a summary of the treatment of the imaging problem in coherence theory. (See p. 11 for examples in which the physical significance of the various parameters is illustrated.)

## BASIC DEFINITIONS

## MUTUAL COHERENCE FUNCTION

The basic entity in the theory of partial coherence is the mutual coherence function  $\Gamma_{12}(\tau)$ , which may be defined by

$$\Gamma_{12}(\tau) \equiv \Gamma(\underline{x}_1, \underline{x}_2, \tau) = \langle V(\underline{x}_1, t) V^*(\underline{x}_2, t + \tau) \rangle . \quad (1)$$

Here the underscore denotes position vector, the asterisk a complex conjugate, and the sharp brackets indicate a long time average,<sup>†</sup> i.e.,

$$\langle f \rangle \equiv \lim_{T \rightarrow \infty} \frac{1}{2T} \int_{-T}^T f dt . \quad (2)$$

---

<sup>†</sup>Equation (2) is equivalent to the definition introduced by Wolf, though in a slightly different form.

In (1)  $V$  is the analytic signal associated with the optical disturbance, which we assume to be a single Cartesian component of the electric field vector. In terms of the mutual coherence function, the complex degree of coherence  $\gamma_{12}(\tau)$  is defined as

$$\gamma_{12}(\tau) = \frac{\Gamma_{12}(\tau)}{\sqrt{\Gamma_{11}(0) \Gamma_{22}(0)}} \quad (3)$$

It should be noted that the complex degree of coherence, like the mutual coherence function, is a function of seven variables, six position coordinates and the time-delay coordinate  $\tau$ . The physical significance of these parameters is illustrated by the example discussed below (p. 11).

The treatment of problems involving partially coherent light involves the solution of the two wave equations:

$$\nabla_s^2 \Gamma_{12}(\tau) = \frac{1}{c} \frac{\partial^2 \Gamma_{12}(\tau)}{\partial \tau^2} \quad (s = 1, 2) \quad (4)$$

where  $\nabla_s^2$  denotes the Laplacian operator in the coordinates of the point  $\mathbf{x}_s$ . A typical problem involves determining the mutual coherence in the source or object plane, solving (4) to obtain the mutual coherence on a later surface such as the image plane, and then recovering the intensity  $I$  in the plane of interest from the relation

$$I(\mathbf{x}_1) = \Gamma(\mathbf{x}_1, \mathbf{x}_1, 0) \quad (5)$$

Equation (5) follows directly from the definition of the mutual coherence function and the properties of the analytic signal.

For a large class of problems the theory outlined in the preceding paragraph may be greatly simplified. These problems are characterized by the quasi-monochromatic approximations, which are stated as

$$\left\{ \begin{array}{l} \Delta \nu < \bar{\nu} \\ |\tau| \ll \frac{1}{\Delta \nu} \end{array} \right\}$$

where  $\Delta\nu$  is the spectral width. Of these two constraints, the second is obviously the more significant. White light may often be treated as quasi-monochromatic if the path differences  $c|\tau|$  involved in the experiment are suitably small. In those circumstances for which the approximations above are applicable, the mutual coherence function may be replaced by the mutual intensity function  $\Gamma(\underline{x}_1, \underline{x}_2)$ :

$$\Gamma(\underline{x}_1, \underline{x}_2) \equiv \Gamma_{12} = \Gamma(\underline{x}_1, \underline{x}_2, 0) \quad (6)$$

The complex degree of coherence reduces to  $\gamma_{12}^{(0)} \equiv \gamma_{12}$  and the wave equations (4) reduce to the two Helmholtz equations

$$\nabla_s^2 \Gamma_{12} + \underline{k}^2 \Gamma_{12} = 0 \quad (s = 1, 2) \quad (7)$$

where  $k$  is the wave number.

#### COHERENT AND INCOHERENT FIELDS

Equations (1) through (7) provide the basis of the theory of partial coherence as introduced by Wolf. To apply this theory to the imaging problem, and recover the familiar limiting forms, several theorems due to Parrent<sup>3</sup> are required. Principal among these are:

1. A field is coherent if and only if the mutual intensity function describing it can be factored in the form

$$\Gamma_{12} = U(\underline{x}_1) U^*(\underline{x}_2) \quad ,$$

where

$$\nabla^2 U(\underline{x}_1) + \underline{k}^2 U(\underline{x}_1) = 0 \quad (8)$$

2. An incoherent field cannot exist in free space; however, an incoherent source consistent with this result may be defined.<sup>4</sup>

(For the proof of these theorems and their extensions to polychromatic fields the reader is referred to Beran and Parrent.<sup>3</sup>) We shall reserve a discussion of the

significance of the incoherent limit for a later point (a comprehensive treatment may be found in Beran and Parrent, Chaps. 2 and 3).

#### THE VAN CITTERT-ZERNIKE THEOREM

The van Cittert-Zernike theorem can also be applied to the image formation problem. It may be stated as follows:

The mutual intensity of the illumination derived from a distant incoherent source may be expressed in the form

$$\Gamma(\underline{x}_1, \underline{x}_2) = \int I(\underline{\xi}) e^{(2\pi i/\lambda R) \underline{\xi} \cdot (\underline{x}_1 - \underline{x}_2)} d\underline{\xi} . \quad (9)$$

Here  $I$  is the intensity distribution across the source, and  $R$  is the distance from the source plane to the observation plane. It is assumed that the observation points  $\underline{x}_1$  and  $\underline{x}_2$  are not far from the optic axis. If the source is placed in the focal plane of a lens and the coherence of the emergent beam examined, Eq. (9) is valid if the  $R$  is replaced by the focal length  $f$ . With this collimating lens, the requirement that the observation points be close to the axis is removed.

#### THE IMAGING PROBLEM

We may now direct our attention to the formulation of the general imaging problem. As will become clear in the following discussion, a basic description of image formation (at least as far as the lenses are concerned) already exists in coherence theory and, in fact, may be found in Refs. 2 and 3. This theory has not however been applied to the significant problems of image evaluation; in fact, it has been applied to very few problems. In the next paragraphs the basic theory is outlined and those pertinent problems that have been solved are reviewed and discussed.

#### REVIEW OF IMAGE THEORY

In coherence theory an object is described by its mutual intensity<sup>†</sup> (or mutual coherence) distribution rather than its intensity distribution. Thus the object is described by  $\Gamma_o(\underline{\xi}_1, \underline{\xi}_2)$  and the relationship between object and image  $\Gamma_i(\underline{x}_1, \underline{x}_2)$  is

<sup>†</sup>Our discussion in this section will be limited to quasi-monochromatic radiation.

developed by solving the two Helmholtz equations (7) subject to the appropriate boundary conditions. The general solution is (see Ref. 3, Chaps. 7 and 8):

$$\Gamma_i(\underline{x}_1, \underline{x}_2) = \iint \Gamma_o(\underline{\xi}_1, \underline{\xi}_2) K(\underline{x}_1 - \underline{\xi}_1) K^*(\underline{x}_2 - \underline{\xi}_2) d\underline{\xi}_1 d\underline{\xi}_2 . \quad (10)$$

Here  $K$  denotes the amplitude impulse response of the lens; i.e., denoting the complex transmission of the aperture by  $A(\underline{\alpha})$ , we may write

$$K(\underline{\xi}) = K\left(\frac{\underline{\beta}}{\lambda f}\right) = \int A(\underline{\alpha}) e^{(2\pi i/\lambda f) \underline{\alpha} \cdot \underline{\beta}} d\underline{\alpha} . \quad (11)$$

The two familiar limits may be recovered from (10) by using the theorems of the previous section. Thus, in the coherent limit  $\Gamma_{12} = U_1 U_2^*$ , and (10) reduces to

$$\Gamma_i(\underline{x}_1, \underline{x}_2) = \int U_o(\underline{\xi}_1) K(\underline{x}_1 - \underline{\xi}_1) d\underline{\xi}_1 \int U_o^*(\underline{\xi}_2) K^*(\underline{x}_2 - \underline{\xi}_2) d\underline{\xi}_2 . \quad (12)$$

From (12) and theorem 1 (p. 6), it is clear that the image of a coherently illuminated object is coherent. A somewhat more surprising result (and certainly more interesting in the image evaluation problem) is obtained in the incoherent limit. Thus, we may take  $\Gamma_{12} = I(\underline{\xi}_1) \delta(\underline{\xi}_1 - \underline{\xi}_2)$  to describe the object.<sup>†</sup> The general image, Eq. (10), then reduces to

$$\Gamma_i(\underline{x}_1, \underline{x}_2) = \int I(\underline{\xi}) K(\underline{x}_1 - \underline{\xi}) K^*(\underline{x}_2 - \underline{\xi}) d\underline{\xi} . \quad (13)$$

From (13) it is clear that the image mutual intensity is no longer of the same form as the object mutual intensity; i.e., the image of an incoherent object is not incoherent but is partially coherent. This result will be seen to have rather far-reaching implications in the problems of image evaluation.

For most applications, the primary exposing radiation may be safely taken as incoherent. For example, sunlight is coherent only over a distance of approximately

<sup>†</sup> Actually this form for the incoherent limit is only an approximation and must be used with care. However, it is sufficiently precise to illustrate the present problem.

1/20 mm. Thus, even a reconnaissance system that resolved an inch on the ground could probably be safely described by the incoherent limit of Eq. (10). In this case, the intensity in the image can be obtained by setting  $\underline{x}_1 = \underline{x}_2$  in (13); thus we write

$$I_i(\underline{x}) = \int I_o(\underline{\xi}) |K(\underline{x} - \underline{\xi})|^2 d\underline{\xi} . \quad (14)$$

Equation (14) will be recognized as the familiar incoherent imaging equation. By taking a Fourier transform of both sides of (14), we obtain the well known relation between object spectrum and image spectrum:

$$\tilde{I}_i(\mu) = \tilde{I}_o(\mu) T(\mu) , \quad (14a)$$

where

$\tilde{I}_i(\mu)$  = Fourier transform of the image intensity distribution

$\tilde{I}_o(\mu)$  = Fourier transform of the object intensity distribution

$T(\mu)$  = transfer function = Fourier transform of the intensity impulse response  $|K(\underline{x})|^2$ .

The relation between object and image is then determined by  $T(\mu)$ , a property of the optical system only. Thus the relation between the object and the image is independent of the particular object used.

Although (10) represents the general solution to the partially coherent imaging problem, a more useful form for application to image analysis is obtained by considering the object to be a transparency that is transilluminated. To describe this class of problems, the object must be described in terms of its complex transmittance  $t(\underline{\xi})$ . For transilluminated objects, Eq. (10) may be expressed as

$$\Gamma_i(\underline{x}_1, \underline{x}_2) = \iint \Gamma_o(\underline{\xi}_1, \underline{\xi}_2) t(\underline{\xi}_1) t^*(\underline{\xi}_2) K(\underline{x}_1 - \underline{\xi}_1) K^*(\underline{x}_2 - \underline{\xi}_2) d\underline{\xi}_1 d\underline{\xi}_2 . \quad (15)$$



In most cases, one is interested in the intensity of the image, which may be obtained from (15) by setting  $\underline{x}_1 = \underline{x}_2$ . Thus,

$$I_i(\underline{x}) = \iint \Gamma_o(\underline{\xi}_1, \underline{\xi}_2) t(\underline{\xi}_1) t^*(\underline{\xi}_2) K(\underline{x} - \underline{\xi}_1) K^*(\underline{x} - \underline{\xi}_2) d\underline{\xi}_1 d\underline{\xi}_2 . \quad (16)$$

The intensity distribution in the image is thus determined by the mutual intensity of the illumination over the object plane, the amplitude impulse response of the optical system, and the amplitude transmittance of the object transparency. In the case where the illumination is derived from a primary incoherent source,  $\Gamma_o(\underline{\xi}_1, \underline{\xi}_2)$  takes a special form (because of the van Cittert-Zernike theorem):

$$\Gamma_o(\underline{\xi}_1, \underline{\xi}_2) \equiv \Gamma_o(\underline{\xi}_1 - \underline{\xi}_2) ; \quad (17)$$

that is, it becomes a function of coordinate differences only. Under these circumstances (16) becomes

$$I_i(\underline{x}) = \iint \Gamma_o(\underline{\xi}_1 - \underline{\xi}_2) t(\underline{\xi}_1) t^*(\underline{\xi}_2) K(\underline{x} - \underline{\xi}_1) K^*(\underline{x} - \underline{\xi}_2) d\underline{\xi}_1 d\underline{\xi}_2 . \quad (18)$$

From (18) it is clear that for transilluminated objects the transition from object intensity  $|t(\underline{\xi})|^2$  to image intensity is nonlinear. The significance of this conclusion is that the customary image evaluation techniques and criteria are not, in general, applicable to such systems. For example, knowing how such a system images sine waves or edges does not permit us to describe how it images other objects. Furthermore, the same optical system could be expected to yield different results if the coherence of the illumination varied. At high resolutions a small variation in the scale of the coherence function can produce dramatic changes in the image.

Since systems of this type are inherently nonlinear, it is impossible to characterize them by a transfer function. This point is easily established by taking the Fourier transform of both sides of (18). Thus,

$$\tilde{I}(\underline{\mu}) = \int \tilde{t}(\underline{\beta}) \tilde{t}^*(\underline{\mu} - \underline{\beta}) \left\{ \int \tilde{\Gamma}[\underline{\mu} - (\underline{\sigma} + \underline{\beta})] \tilde{K}(\underline{\mu} - \underline{\sigma}) \tilde{K}^*(\underline{\sigma}) d\underline{\sigma} \right\} d\underline{\beta} . \quad (19)$$

In (19) the inner integral is characteristic of the instrument and the illumination; on the other hand, the factors  $\tilde{t}(\beta)$  and  $\tilde{t}^*(\underline{u} - \beta)$  are determined solely from the object spectrum. However, (19) is not in the form of "object spectrum times transfer function equals image spectrum" as Eq. (14a) is. Therefore, with partially coherent illumination the relation between object and image is different for each object. It is also evident that with partially coherent illumination the object-image relation is a relation between object amplitude transmittance and image intensity. The inner integral has been referred to as a generalized transfer function, but that nomenclature is rather misleading since the function is not used as a transfer function at all. A better terminology is the more cumbersome one introduced by Wolf, the "transmission cross coefficient," which emphasizes that it is a function of two frequencies.

Although the preceding analysis provides a basis or structure for the complete description of partially coherent imaging systems, it is formidable enough to make intuitive interpretation rather difficult. Therefore, to gain some insight into the significance of these developments in image evaluation, some examples will now be given.

#### EXAMPLES OF PARTIALLY COHERENT IMAGING

We shall apply the theory developed in the preceding section to the description of two typical experiments that might be used to "measure the transfer function of an imaging system" — imaging of cosine targets and the edge trace method.

##### Cosine Targets

First let us consider the approach of direct imaging of cosine targets. The experimental arrangement is illustrated schematically in Figure 2. Here a source

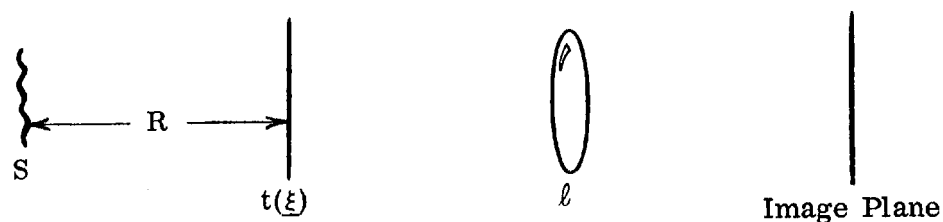


Figure 2. Direct Imaging of Cosine Targets

S is located R units to the left of a transparency  $t(\xi)$ , which is then imaged by the lens  $\ell$  onto the image plane. For simplicity, we will assume unit magnification. The nature of our calculation will be such that the results are equally applicable for all R and for the case where a lens is used to collimate the source onto  $t(\xi)$ . Since the radiation will be partially coherent, it is necessary to describe the experiment very carefully. We shall be interested in calculating the ratio of the image modulation in terms of intensity to the object modulation, also measured in intensity. This modulation ratio will, of course, be identical with the transfer function in the incoherent limit, but otherwise it will be an apparent transfer function describing the result of the measurement of cosine waves and of little or no use in describing the measurement of other objects.

To formally solve the problem, the complex transmittance of the object must be specified. To avoid the complexity of phase objects, we shall consider the transmittance to be of the form

$$t(\xi) = 1 + \cos 2\pi\mu_o \xi . \quad (20)$$

(Here, and throughout this section, we limit our analysis to one dimension.) The corresponding intensity in the object is

$$|t(\xi)|^2 = \frac{3}{2} + 2 \cos 2\pi\mu_o \xi + \frac{1}{2} \cos 2\pi 2\mu_o \xi . \quad (21)$$

The resulting image will be shown to be an intensity function of the form

$$I(x) = A + B \cos 2\pi\mu_o \xi + C \cos 2\pi 2\mu_o \xi , \quad (22)$$

where, of course, A, B, and C are yet to be determined. The modulation in the image divided by the modulation in the object will be plotted versus  $\mu_o$ . As a result

of the nonlinearities, the modulation ratios for  $\mu_0$  and  $2\mu_0$  will not lead to the same apparent transfer functions. To begin, rearrange the integral in (19) to the form

$$\tilde{I}(\mu) = \int \tilde{K}(\mu - \sigma) \tilde{K}^*(\sigma) \left\{ \int \tilde{t}(\beta) \tilde{t}^*(\mu - \beta) \tilde{\Gamma}[\mu - (\sigma + \beta)] d\beta \right\} d\sigma. \quad (23)$$

Consider the inner integral in (23), i.e.,

$$\mathcal{J}(\mu, \sigma) = \int \tilde{t}(\beta) \tilde{t}^*(\mu - \beta) \tilde{\Gamma}[\mu - (\sigma + \beta)] d\beta \quad (24)$$

and note that

$$\tilde{t}(\beta) = \delta(\beta) + \frac{1}{2} \delta(\beta - \mu_0) + \frac{1}{2} \delta(\beta + \mu_0). \quad (25)$$

Then

$$\tilde{t}(\mu - \beta) = \delta(\mu - \beta) + \frac{1}{2} \delta(\mu - \beta - \mu_0) + \frac{1}{2} \delta(\mu - \beta + \mu_0). \quad (26)$$

Using (25) and (26) we obtain for Eq. (24):

$$\begin{aligned} \mathcal{J}(\mu, \sigma) = \int \tilde{\Gamma}[\mu - (\sigma + \beta)] & \left\{ \delta(\beta) + \frac{1}{2} \delta(\beta - \mu_0) + \frac{1}{2} \delta(\beta + \mu_0) \right\} \\ & \times \left\{ \delta(\mu - \beta) + \frac{1}{2} \delta(\mu - \beta - \mu_0) + \frac{1}{2} \delta(\mu - \beta + \mu_0) \right\} d\beta \end{aligned} \quad (27)$$

or

$$\begin{aligned} \mathcal{J}(\mu, \sigma) = \tilde{\Gamma}(\mu - \sigma) & \left\{ \delta(\mu) + \frac{1}{2} \delta(\mu - \mu_0) + \frac{1}{2} \delta(\mu + \mu_0) \right\} \\ & + \frac{1}{2} \tilde{\Gamma}[\mu - (\sigma + \mu_0)] \left\{ \delta(\mu - \mu_0) + \frac{1}{2} \delta(\mu - 2\mu_0) + \frac{1}{2} \delta(\mu) \right\} \\ & + \frac{1}{2} \tilde{\Gamma}[\mu - (\sigma - \mu_0)] \left\{ \delta(\mu + \mu_0) + \frac{1}{2} \delta(\mu) + \frac{1}{2} \delta(\mu + 2\mu_0) \right\}. \end{aligned} \quad (28)$$

Substituting from (28) into (23) yields

$$I(x) = \int \int \mathcal{A}(\mu, \sigma) \tilde{K}(\mu - \sigma) \tilde{K}^*(\sigma) d\sigma e^{2\pi i \mu x} d\mu \quad (29)$$

$$= \int G(\sigma, x) \tilde{K}^*(\sigma) d\sigma, \quad (30)$$

where

$$G(\sigma, x) = \int \mathcal{A}(\mu, \sigma) \tilde{K}(\mu - \sigma) e^{2\pi i \mu x} d\mu. \quad (31)$$

Equation (31) may be integrated to yield

$$\begin{aligned} G(\sigma, x) = & \tilde{\Gamma}(-\sigma) \tilde{K}(-\sigma) + \frac{e^{2\pi i \mu_0 x}}{2} \left[ \tilde{\Gamma}(\mu_0 - \sigma) \tilde{K}(\mu_0 - \sigma) + \tilde{\Gamma}(-\sigma) \tilde{K}(\mu_0 - \sigma) \right] \\ & + \frac{e^{-2\pi i \mu_0 x}}{2} \left[ \tilde{\Gamma}(-\mu_0 - \sigma) \tilde{K}(-\mu_0 - \sigma) + \tilde{\Gamma}(-\sigma) \tilde{K}(-\mu_0 - \sigma) \right] \\ & + \frac{e^{2\pi i 2\mu_0 x}}{4} \left[ \tilde{\Gamma}(\mu_0 - \sigma) \tilde{K}(2\mu_0 - \sigma) \right] + \frac{1}{4} e^{-2\pi i 2\mu_0 x} \left[ \tilde{\Gamma}(-\sigma - \mu_0) \tilde{K}(-2\mu_0 - \sigma) \right] \\ & + \frac{1}{4} \left[ \tilde{\Gamma}(-\sigma - \mu_0) \tilde{K}(-\sigma) + \tilde{\Gamma}(-\sigma + \mu_0) \tilde{K}(-\sigma) \right]. \end{aligned} \quad (32)$$

Substituting from (32) into (30) we obtain

$$\begin{aligned} I(x) = & \int \tilde{\Gamma}(-\sigma) \tilde{K}(-\sigma) \tilde{K}(\sigma) d\sigma + \frac{1}{4} \int \tilde{K}(\sigma) \left[ \tilde{\Gamma}(-\sigma - \mu_0) \tilde{K}(-\sigma) + \tilde{\Gamma}(-\sigma + \mu_0) \tilde{K}(-\sigma) \right] d\sigma \\ & + \int \left[ \tilde{\Gamma}(\mu_0 - \sigma) \tilde{K}(\mu_0 - \sigma) + \tilde{\Gamma}(-\sigma) \tilde{K}(\mu_0 - \sigma) \right] \tilde{K}(\sigma) d\sigma \cos \left[ 2\pi \mu_0 x \right] \\ & + \frac{1}{2} \int \tilde{\Gamma}(\mu_0 - \sigma) \tilde{K}(2\mu_0 - \sigma) \tilde{K}(\sigma) d\sigma \cos \left[ 2\pi 2\mu_0 x \right] \\ = & I_1 + I_2 + I_3 \cos 2\pi \mu_0 x + I_4 \cos 2\pi 2\mu_0 x. \end{aligned} \quad (33)$$

Equation (33) represents the general solution for the imaging of cosine waves with partially coherent light. To emphasize the coherence effects and avoid the complications of aberrated optics, the restriction to diffraction-limited lenses has been imposed. Thus, the aperture function  $A(x)$  is given by

$$A(x) = \begin{cases} 1, & |x| \leq \alpha \\ 0, & |x| > \alpha \end{cases} . \quad (34)$$

The corresponding impulse response is of course

$$\begin{aligned} K(\xi) &= \int A(x) e^{\frac{2\pi i \xi x}{\lambda f}} dx \\ &= 2\alpha \operatorname{sinc} \frac{2\pi \alpha x}{\lambda f} . \end{aligned} \quad (35)$$

The Fourier transform of the impulse response is thus

$$\tilde{K}(\sigma) = \begin{cases} 1, & |\sigma| \leq \frac{\alpha}{\lambda f} \\ 0, & |\sigma| > \frac{\alpha}{\lambda f} \end{cases} = \begin{cases} 1, & |\sigma| \leq a \\ 0, & |\sigma| > a \end{cases} . \quad (36)$$

Equation (36) serves to define the parameter  $a$ . Let us further assume that the radiation is derived from a primary incoherent source of width  $2\eta$ . Then by the van Cittert-Zernike theorem, the mutual intensity is given by

$$\Gamma(\xi_1, \xi_2) = \int_{-\eta}^{\eta} e^{2\pi i x(\xi_1 - \xi_2)} dx = 2\eta \operatorname{sinc} 2\pi\eta(\xi_1 - \xi_2) . \quad (37)$$

Thus, the Fourier transform of the mutual intensity is

$$\tilde{\Gamma}(\sigma) = \begin{cases} 1, & |\sigma| \leq \frac{\eta}{\lambda f} \\ 0, & |\sigma| > \frac{\eta}{\lambda f} \end{cases} = \begin{cases} 1, & |\sigma| \leq b \\ 0, & |\sigma| > b \end{cases} . \quad (38)$$

Equation (38) can serve to define the parameter  $b$ . Using (38) and (36), we may evaluate (33) to yield

$$\begin{aligned}
 I_1 &= 2 \left\{ \begin{matrix} a \\ b \end{matrix} \right\} \\
 I_2 &= \frac{1}{2} \left\{ \begin{matrix} 0 & \mu_o > a + b \\ a + b - \mu_o & b - a < \mu_o < b + a \text{ and } \mu_o > a - b \\ 2a & a - b < \mu_o < b - a \\ 2b & b - a < \mu_o < a - b \end{matrix} \right\} \\
 I_3 &= 2 \left\{ \begin{matrix} 0 & \mu_o > 2a \text{ or } \mu_o > a + b \\ a + b - \mu_o & a > b \text{ and } a - b < \mu_o < a + b \\ 2b & a > b \text{ and } 0 < \mu_o < a - b \\ 2a - \mu_o & a < b \text{ and } 0 < \mu_o < 2a \end{matrix} \right\} \\
 I_4 &= \frac{1}{2} \left\{ \begin{matrix} 0 & \mu_o > a \\ 2b & a > b \text{ and } 0 < \mu_o < a - b \\ 2a - 2\mu_o & a - b < \mu_o < a \end{matrix} \right\}
 \end{aligned} \tag{39}$$

Here the symbol  $\left\{ \begin{matrix} a \\ b \end{matrix} \right\}$  is to be read "a or b, whichever is smaller."

Using (39) we can plot the modulation ratio versus the line frequency of the original target. This parameter is given by

$$C(\mu_o) = \frac{3}{4} \left[ \frac{I_3}{I_1 + I_2} \right] \tag{40}$$

The modulation ratio versus line frequency is plotted in Figure 3. If the system were linear, the same modulation ratio curves should be obtained for the second harmonic term. This, however, is not the case and the difference is shown in Figure 4. Furthermore, the curves here only apply for unit modulation targets. Since the system is nonlinear the apparent transfer function varies with the modulation of the target.

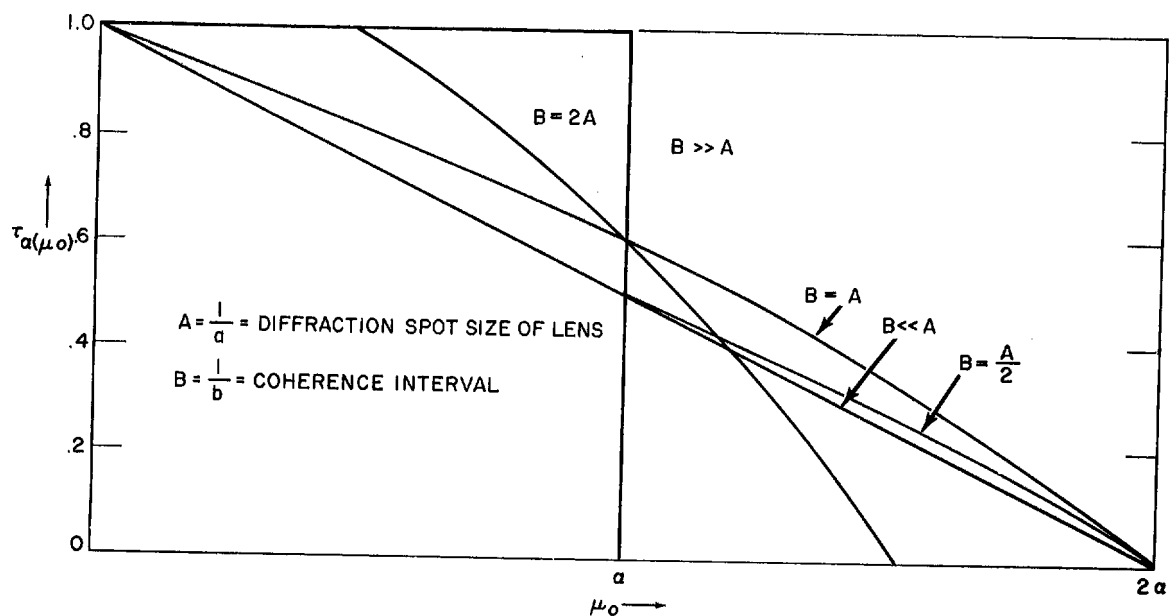


Figure 3. Apparent Transfer Function Measured for Fundamental Term of Sine Wave Targets

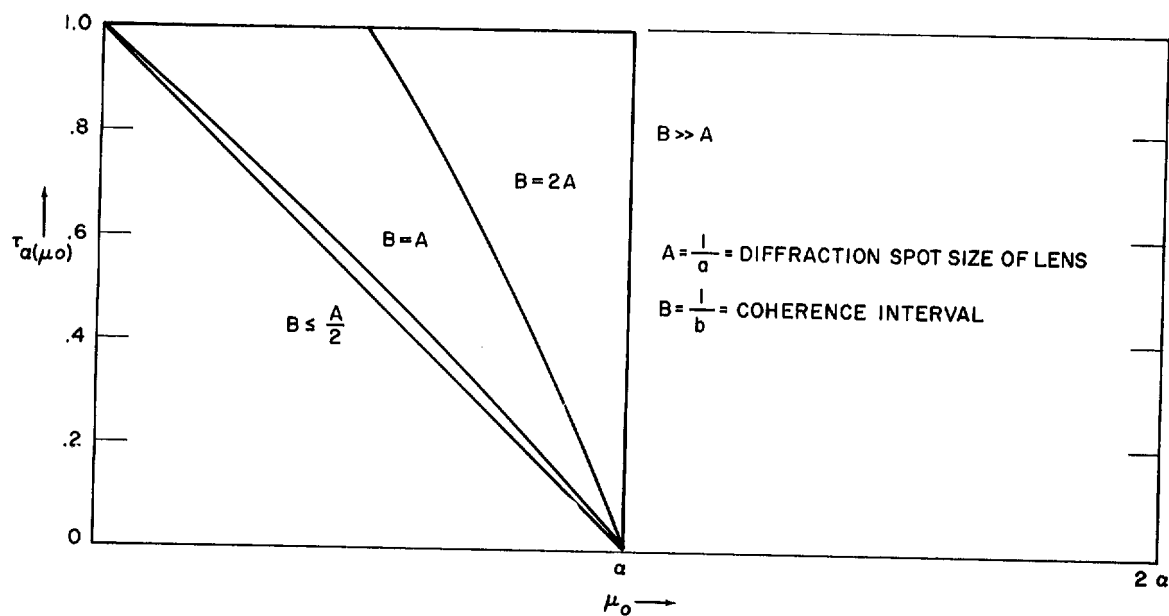


Figure 4. Apparent Transfer Function for Second Harmonic Term



Edge Objects

Briefly, the edge trace method may be summarized as follows. For a stationary linear system with impulse response  $s(x)$ , the image of an edge is given by

$$I(x) = \int_{-\infty}^{\infty} E(x') s(x - x') dx' , \quad (41)$$

where  $E(x)$  describes the edge, i. e. ,

$$E(x) = \frac{1}{2} + \frac{1}{2} \operatorname{sgn}(x) . \quad (42)$$

The Fourier transform of  $I(x)$  is, of course,

$$\begin{aligned} \tilde{I}(\mu) &= \tilde{E}(\mu) \tilde{s}(\mu) \\ &= \frac{1}{2} \left[ \delta(\mu) - \frac{i}{\pi\mu} \right] \tilde{s}(\mu) . \end{aligned} \quad (43)$$

Multiplying both sides of (43) by  $2\pi i\mu$  and taking the Fourier transform yields

$$\int 2\pi i\mu \tilde{I}(\mu) e^{2\pi i\mu x} d\mu = \pi i \int \mu \delta(\mu) \tilde{s}(\mu) e^{2\pi i\mu x} d\mu + \int \tilde{s}(\mu) e^{2\pi i\mu x} d\mu . \quad (44)$$

The first integral on the right of (44) vanishes, leaving

$$\int 2\pi i\mu \tilde{I}(\mu) e^{2\pi i\mu x} d\mu = s(x) . \quad (45)$$

Or, taking the inverse transform, we have

$$\tilde{s}(\mu) = 2\pi i\mu \tilde{I}(\mu) . \quad (46)$$

This method is widely used in the determination of the transfer function  $\tilde{s}(\mu)$ . The approach in this section will be to carry through the calculations indicated in (41) through (46) for partially coherent light. The result will, of course, not be interpretable as a transfer function, but it will correspond to an apparent transfer function; that is, it will describe the result on an edge-trace experimental program.

For the present problem, the transmittance of the object will be

$$t(x) = \frac{1}{2} + \frac{1}{2} \operatorname{sgn} x \quad (47)$$

and its spectrum is

$$\tilde{t}(\beta) = \frac{1}{2} \left[ \delta(\beta) - \frac{iP}{\pi\beta} \right], \quad (48)$$

where  $P$  is to be interpreted as the principal part operator if  $\tilde{t}$  occurs in an integration. Following the same procedure as before, we substitute Eq. (48), which results in an inner integral of the form

$$\begin{aligned} \mathcal{J}(\sigma, \mu) &= \int \tilde{t}(\beta) \tilde{t}(\mu - \beta) \tilde{\Gamma}[\mu - (\sigma + \beta)] d\beta \\ &= I_1 + I_2 + I_3 + I_4 \end{aligned} \quad (49)$$

where

$$\begin{aligned} I_1(\sigma, \mu) &= \frac{1}{4} \int \delta(\beta) \delta(\mu - \beta) \tilde{\Gamma}[\mu - (\sigma + \beta)] d\beta \\ &= \frac{1}{4} \delta(\mu) \tilde{\Gamma}(\mu - \sigma); \end{aligned} \quad (50)$$

$$\begin{aligned} I_2(\sigma, \mu) &= -\frac{1}{4} \frac{iP}{\pi} \int \frac{\delta(\mu - \beta)}{\beta} \tilde{\Gamma}[\mu - (\sigma + \beta)] d\beta \\ &= -\frac{1}{4} \frac{iP}{\pi} \frac{\tilde{\Gamma}(-\sigma)}{\mu}; \end{aligned} \quad (51)$$

$$\begin{aligned}
 I_3(\sigma, \mu) &= -\frac{iP}{4\pi} \int \frac{\delta(\beta)}{\mu - \beta} \tilde{\Gamma} \left[ \mu - (\sigma + \beta) \right] d\beta \\
 &= -\frac{iP}{4\pi} \frac{\tilde{\Gamma}(\mu - \sigma)}{\mu} ;
 \end{aligned} \tag{52}$$

$$I_4(\sigma, \mu) = -\frac{P}{4\pi^2} \oint \frac{\tilde{\Gamma}[\mu - (\sigma + \beta)]}{(\mu - \beta)} d\beta . \tag{53}$$

To evaluate  $I_4(\sigma, \mu)$ , recall that

$$\tilde{\Gamma}(\nu) = \begin{cases} 1, & |\nu| \leq b \\ 0, & |\nu| > b \end{cases} ;$$

hence

$$\begin{aligned}
 I_4(\sigma, \mu) &= -\frac{P}{4\pi^2} \oint_{\mu - (\sigma - b)}^{\mu - (\sigma + b)} \frac{d\beta}{\beta(\mu - \beta)} \\
 &= -\frac{P}{4\pi^2} \left[ \frac{1}{\mu} \int_{\mu - \sigma + b}^{\mu - \sigma - b} \frac{d\beta}{\beta} + \frac{1}{\mu} \int_{\mu - \sigma + b}^{\mu - \sigma - b} \frac{d\beta}{\mu - \beta} \right] \\
 &= -\frac{1}{4\pi^2 \mu} \lim_{\epsilon \rightarrow 0} \left[ \int_{\mu - \sigma + b}^{-\epsilon} \frac{d\beta}{\beta} + \int_{\epsilon}^{\mu - \sigma - b} \frac{d\beta}{\beta} + \int_{\mu - \sigma + b}^{\mu - \epsilon} \frac{d\beta}{\mu - \beta} + \int_{\mu + \epsilon}^{\mu - \sigma - b} \frac{d\beta}{\mu - \beta} \right] \\
 &= -\frac{1}{4\pi^2 \mu} \ln \left[ \frac{(\mu - \sigma - b)(\sigma - b)}{(\mu - \sigma + b)(\sigma + b)} \right] .
 \end{aligned} \tag{54}$$

Then using (50), (51), (52), and (54), we have

$$\begin{aligned}
 \tau_a(\mu) = & 2\pi i \mu \left\{ \frac{1}{4} \int \delta(\mu) \tilde{\Gamma}(\mu - \sigma) \tilde{K}(\mu - \sigma) \tilde{K}(\sigma) d\sigma \right. \\
 & - \frac{1}{4} \frac{iP}{\pi} \int \frac{\tilde{\Gamma}(\sigma)}{\mu} \tilde{K}(\mu - \sigma) \tilde{K}(\sigma) d\sigma \\
 & - \frac{iP}{4\pi} \int \frac{\tilde{\Gamma}(\mu - \sigma)}{\mu} \tilde{K}(\mu - \sigma) \tilde{K}(\sigma) d\sigma \\
 & \left. - \frac{1}{4\pi} \frac{2}{\mu} \int \ln \left[ \frac{(\mu - \sigma - b)(\sigma - b)}{(\mu - \sigma + b)(\sigma + b)} \right] \tilde{K}(\mu - \sigma) \tilde{K}(\sigma) d\sigma \right\} .
 \end{aligned} \tag{55}$$

The first integral is zero because  $\mu\delta(\mu) = 0$ . By a change of variables it can be shown that the second and third integrals are equal. Thus, we have

$$\begin{aligned}
 \tau_a(\mu) = & \int \tilde{\Gamma}(\sigma) \tilde{K}(\mu - \sigma) \tilde{K}(\sigma) d\sigma \\
 & - \frac{i}{2\pi} \int \ln \left[ \frac{(\mu - \sigma - b)(\sigma - b)}{(\mu - \sigma + b)(\sigma + b)} \right] \tilde{K}(\mu - \sigma) \tilde{K}(\sigma) d\sigma .
 \end{aligned} \tag{56}$$

Again, limiting our attention to diffraction-limited lenses and incoherent primary sources, we may evaluate the two integrals in (56) to yield

$$\begin{aligned}
 \tau_a(\mu) = & \left\{ \begin{array}{ll} 0 & \mu > 2a \text{ or } \mu > a + b \\ a + b - \mu & a > b \text{ and } \mu > b - a \\ 2a - \mu & b > a \text{ and } 0 < \mu < 2a \\ 2b & b < a \text{ and } b - a < \mu < a - b \end{array} \right\} \\
 & - \frac{i}{\pi} \left\{ \ln \left[ \frac{(a - b)^{(a - b)}}{(a + b)^{(a + b)}} \frac{(\mu - a + b)^{(\mu - a + b)}}{(\mu - a - b)^{(\mu - a - b)}} \right] \right\} .
 \end{aligned} \tag{57}$$

The expression in Eq. (57) describes the apparent or measured transfer function obtained by edge-trace analysis for a diffraction-limited system. One notices immediately that this function is complex. Thus, even though the system impulse response (for coherent or incoherent light) is symmetric, the measured apparent transfer function will be complex; i.e., it will exhibit non-zero phase shifts. A plot of this apparent transfer function for various values of the ratio of diffraction spot to coherence interval is plotted in Figure 5. The second point that is immediately clear from these curves is that the apparent transfer function is different even in magnitude from the result obtained using sine waves. It should be noted that in both cases the curves deviate significantly from the expected values in the neighborhood of  $a = b$ . This treatment of the partially coherent imaging situation in terms of the "apparent transfer function" for a particular object will be used again in Chapter 5 to find the effects of coherence on the frequency content of certain targets.

25X1

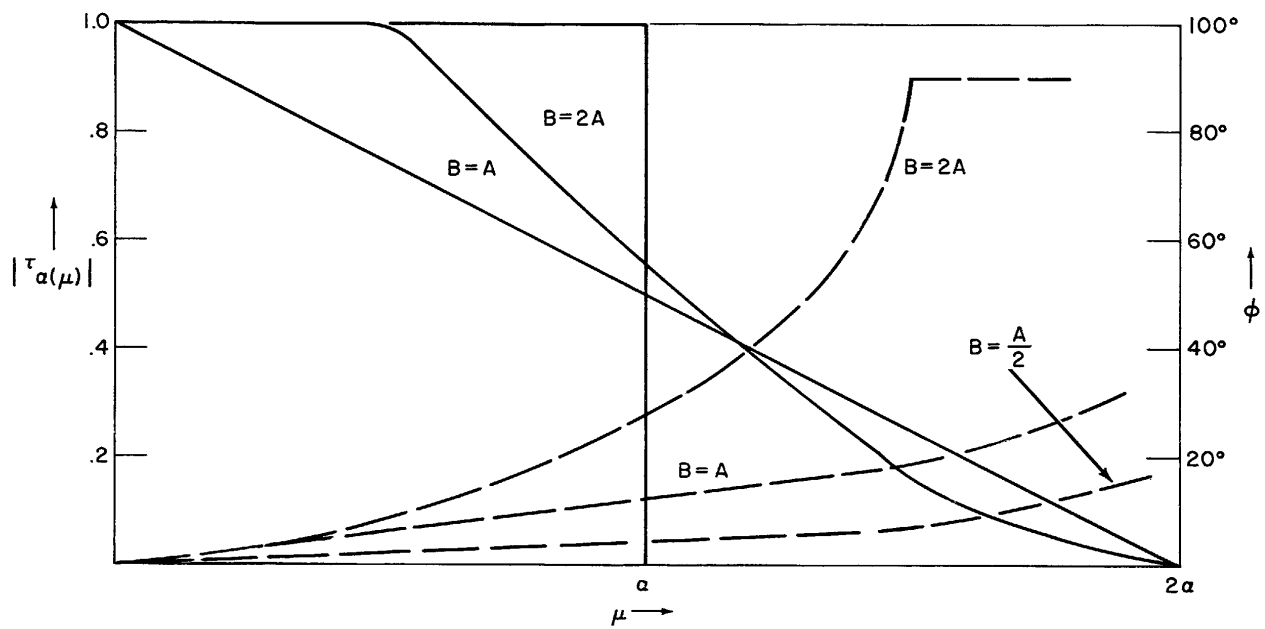


Figure 5. Apparent Transfer Function from an Edge Trace

25X1

## CHAPTER 3

## DEGREE OF COHERENCE IN THE OBJECT PLANE

We showed in Chapter 2 that when an object is illuminated by partially coherent quasi-monochromatic light and we want to predict the intensity distribution in the image of that object, we must first determine  $\Gamma_o(\xi_1, \xi_2)$ , the mutual intensity distribution in the object plane. This dependence of the image intensity distribution  $I_i(x)$  on  $\Gamma_o(\xi_1, \xi_2)$  was expressed by Eq. (16). In this chapter, we present the theoretical and experimental determination of  $\Gamma_o(\xi_1, \xi_2)$ .

Essential elements of the illumination system were shown in Figure 1. The laser emits (when operated in single mode) an approximately plane quasi-monochromatic wave with a Gaussian intensity distribution across the beam. This intensity distribution was measured experimentally; its measured values are compared with a Gaussian function in Figure 6. A condenser lens is used to direct this beam onto a moving piece of ground glass, which scatters the laser light in such a way that the average intensity distribution in the object plane  $\xi$  is approximately constant over a large part of the format area centered on the optical axis. A collimating lens is used between the rotating ground glass and the object plane.

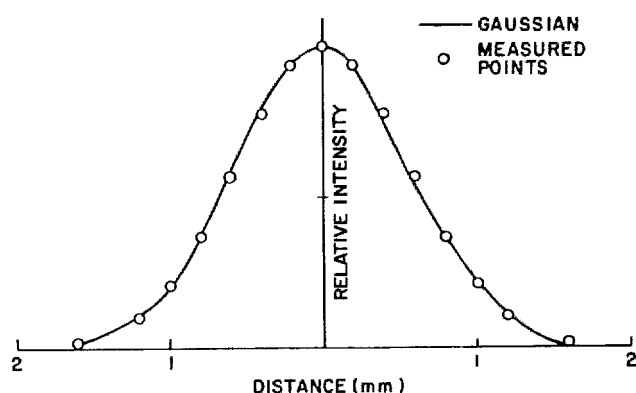


Figure 6. Intensity Across Single Mode Laser Beam vs Gaussian of Halfwidth 0.8 mm

The problem of determining  $\Gamma_o(\xi_1, \xi_2)$  in the object plane is then essentially one of finding the effect of the moving ground glass on the spatial coherence of the laser light.

## THEORETICAL PREDICTION

Here we will use statistical considerations to derive the expression for  $\overline{\Gamma_o(\xi_1, \xi_2)}$ , the ensemble-averaged mutual intensity distribution in the object plane. The members

of the ensemble over which we average are the particular configurations of the ground glass disc. By assuming that ensemble and time averages are equivalent,

we will then identify  $\overline{\Gamma_o(\xi_1, \xi_2)}$  with the time-averaged mutual intensity distribution to be expected in the object plane. (At the end of this chapter we show the excellent agreement between this theoretical prediction and the experimental measurements.)

We found in Eq. (15) that for transilluminated objects the mutual intensity distribution in the image plane is of the form

$$\Gamma_i(\underline{x}_1, \underline{x}_2) = \iint \Gamma_o(\underline{\xi}_1, \underline{\xi}_2) t(\underline{\xi}_1) t^*(\underline{\xi}_2) K(\underline{x}_1 - \underline{\xi}_1) K^*(\underline{x}_2 - \underline{\xi}_2) d\underline{\xi}_1 d\underline{\xi}_2 . \quad (58)$$

However, no constraint to imaging situations was imposed on the derivation of (58), and in fact the same equation applies to the more general problem of propagating from any plane surface to another plane surface. The form of  $K(\underline{x} - \underline{\xi})$  will of course change accordingly. For the problem of propagation from the plane  $\underline{\alpha}$  of the ground glass to the plane  $\underline{\xi}$  of the object, Eq. (58) will then become

$$\Gamma_o(\underline{\xi}_1, \underline{\xi}_2) = \iint \Gamma_G(\underline{\alpha}_1, \underline{\alpha}_2) t(\underline{\alpha}_1) t^*(\underline{\alpha}_2) K(\underline{\xi}_1 - \underline{\alpha}_1) K(\underline{\xi}_2 - \underline{\alpha}_2) d\underline{\alpha}_1 d\underline{\alpha}_2 , \quad (59)$$

where  $\Gamma_G(\underline{\alpha}_1, \underline{\alpha}_2)$  is the mutual intensity of the laser light incident on the ground glass,  $t(\underline{\alpha})$  is the complex amplitude transmittance of the ground glass, and  $K(\underline{\xi})$  is the amplitude response in the object plane from a point source in the plane of the ground glass. In each configuration or position of the ground glass disc, a long time average as required by (1) will take place. During the time of an exposure the moving ground glass will pass through a great many of these configurations. Thus we are interested in an average of  $\Gamma_o(\underline{\xi}_1, \underline{\xi}_2)$  over the ensemble of configurations. We denote this by  $\overline{\Gamma_o(\underline{\xi}_1, \underline{\xi}_2)}$ . The quantity of interest is then

$$\overline{\Gamma_o(\underline{\xi}_1, \underline{\xi}_2)} = \iint \Gamma_G(\underline{\alpha}_1, \underline{\alpha}_2) t(\underline{\alpha}_1) t^*(\underline{\alpha}_2) K(\underline{\xi}_1 - \underline{\alpha}_1) K(\underline{\xi}_2 - \underline{\alpha}_2) d\underline{\alpha}_1 d\underline{\alpha}_2 . \quad (60)$$

The amplitude impulse response  $K(\underline{\xi})$  and the mutual intensity  $\Gamma_G(\underline{\alpha}_1, \underline{\alpha}_2)$  may be considered to be independent of the configuration of the ground glass; therefore Eq. (60) becomes

$$\overline{\Gamma_o(\underline{\xi}_1, \underline{\xi}_2)} = \iint \Gamma_G(\underline{\alpha}_1, \underline{\alpha}_2) \overline{t(\underline{\alpha}_1) t^*(\underline{\alpha}_2)} K(\underline{\xi}_1 - \underline{\alpha}_1) K(\underline{\xi}_2 - \underline{\alpha}_2) d\underline{\alpha}_1 d\underline{\alpha}_2 . \quad (61)$$



The amplitude transmittance  $t(\underline{\alpha})$  of the ground glass will have the form

$$t(\underline{\alpha}) = e^{ik\Delta(\underline{\alpha})}, \quad (62)$$

where  $k = 2\pi/\lambda$ , and  $\Delta(\underline{\alpha})$  = the thickness of the ground glass disc. Thus, since the only effect of the glass thickness is to change the phase of the incident light, we then write

$$\overline{t(\underline{\alpha}_1) t^*(\underline{\alpha}_2)} = e^{\overline{ik [\Delta(\underline{\alpha}_1) - \Delta(\underline{\alpha}_1 - \underline{\epsilon})]}}, \quad (63)$$

where  $\underline{\epsilon} = \underline{\alpha}_1 - \underline{\alpha}_2$ . To evaluate the right-hand side of (63), some assumption about the statistics of the glass surface roughness must be made at this point in the derivation. A reasonable assumption, and a useful one from the viewpoint of computation, is that the glass thickness is a Gaussianly distributed random variable with zero mean, variance  $\sigma^2$ , and an autocorrelation function of the form

$$\phi(\underline{\epsilon}) = \overline{\Delta(\underline{\alpha}_1) \Delta(\underline{\alpha}_1 - \underline{\epsilon})}. \quad (64)$$

O'Neill<sup>5</sup> has evaluated Eq. (63) and shown that for this case

$$\overline{t(\underline{\alpha}_1) t^*(\underline{\alpha}_2)} = e^{-k^2 [\sigma^2 - \phi(\underline{\epsilon})]}. \quad (65)$$

The ensemble-averaged quantity  $\overline{t(\underline{\alpha}_1) t^*(\underline{\alpha}_2)}$  therefore depends only on the variance  $\sigma^2$  and autocorrelation function  $\phi(\underline{\epsilon})$  of the ground glass thickness. Using (65), we rewrite (61) as

$$\overline{\Gamma_o(\underline{\xi}_1, \underline{\xi}_2)} = e^{-k^2 \sigma^2} \iint \Gamma_G(\underline{\alpha}_1, \underline{\alpha}_2) e^{k^2 \phi(\underline{\epsilon})} K(\underline{\xi}_1 - \underline{\alpha}_1) K^*(\underline{\xi}_2 - \underline{\alpha}_2) d\underline{\alpha}_1 d\underline{\alpha}_2. \quad (66)$$

The next task in evaluating (66) is specification of  $\Gamma_G(\underline{\alpha}_1, \underline{\alpha}_2)$  and  $K(\underline{\xi} - \underline{\alpha})$ . By considering the basic propagation problem, it can easily be shown that the effect

of the collimating lens is to put the object plane in the far field of the ground glass. Thus we may take

$$K(\underline{\xi} - \underline{\alpha}) = e^{(ik/f)(\underline{\xi} \cdot \underline{\alpha})} , \quad (67)$$

where  $f$  is the focal length of the collimating lens. To specify  $\Gamma_G(\underline{\alpha}_1, \underline{\alpha}_2)$  we use theorem 1 of Chapter 2. A field is coherent if and only if the mutual intensity function describing it can be factored in the form

$$\Gamma_G(\underline{\alpha}_1, \underline{\alpha}_2) = U_G(\underline{\alpha}_1) U_G^*(\underline{\alpha}_2) . \quad (68)$$

By assumption, the laser light incident on the ground glass is coherent and thus  $\Gamma_G(\underline{\alpha}_1, \underline{\alpha}_2)$  must factor as in (68). However, the amplitude cannot be determined uniquely from an intensity distribution. We must, therefore, assume a certain form for  $U(\underline{\alpha}_1)$  in (68), subject to the condition that the intensity of this radiation incident on the ground glass have the Gaussian form shown in Figure 6. Thus we take

$$\Gamma_G(\underline{\alpha}_1, \underline{\alpha}_2) = e^{-(c/2)\underline{\alpha}_1^2} e^{-(c/2)\underline{\alpha}_2^2} . \quad (69)$$

The intensity  $I_G(\underline{\alpha})$  of the light defined as in Eq. (5) can then be seen to be Gaussian. The constant  $c$  in (69) is determined from Figure 6.

Using (67) and (69), we rewrite (66) as

$$\overline{\Gamma_o(\underline{\xi}_1, \underline{\xi}_2)} = \iint e^{-(c/2)\left(\underline{\alpha}_1^2 + \underline{\alpha}_2^2\right)} e^{k^2 \phi(\underline{\alpha}_1 - \underline{\alpha}_2)} e^{(ik/f)(\underline{\xi}_1 \cdot \underline{\alpha}_1 - \underline{\xi}_2 \cdot \underline{\alpha}_2)} d\underline{\alpha}_1 d\underline{\alpha}_2 , \quad (70)$$

where we have used  $\underline{\epsilon} = \underline{\alpha}_1 - \underline{\alpha}_2$  and dropped the constant factor  $e^{-k^2 \sigma^2}$  since it is of no consequence for this calculation.

Now we use the Fourier transforms

$$e^{-(c/2)\underline{\alpha}_2^2} = \int_{-\infty}^{\infty} e^{-(1/2c)\underline{\mu}'^2} e^{2\pi i \underline{\mu}' \cdot \underline{\alpha}_2} d\underline{\mu}' \quad (71)$$

and

$$e^{k^2 \phi(\underline{\alpha}_1 - \underline{\alpha}_2)} = \int_{-\infty}^{\infty} F(\underline{\mu}) e^{2\pi i \underline{\mu} \cdot (\underline{\alpha}_1 - \underline{\alpha}_2)} d\underline{\mu} \quad (72)$$

Equation (72) is just a definition of  $F(\underline{\mu})$ . When (71) and (72) are substituted into (70), Eq. (70) becomes

$$\begin{aligned} \overline{\Gamma_o(\underline{x}_1, \underline{x}_2)} = \int e^{-(c/2)\underline{\alpha}_1^2} & \left[ \iint e^{-(1/2c)\underline{\mu}'^2} F(\underline{\mu}) e^{2\pi i \underline{\mu}' \cdot \underline{\alpha}_2} \right. \\ & \left. e^{2\pi i \underline{\mu} \cdot (\underline{\alpha}_1 - \underline{\alpha}_2)} e^{(2\pi i/\lambda)\underline{x}_2 \cdot \underline{\alpha}_2} d\underline{\alpha}_2 d\underline{\mu} d\underline{\mu}' \right] e^{(2\pi i/\lambda)\underline{x}_1 \cdot \underline{\alpha}_1} d\underline{\alpha}_1 \quad (73) \end{aligned}$$

Since the integral over  $\underline{\alpha}_2$  is a  $\delta$  function, Eq. (73) becomes

$$\begin{aligned} \overline{\Gamma_o(\underline{x}_1, \underline{x}_2)} = \int e^{-(c/2)\underline{\alpha}_1^2} & \left[ \iint e^{-(1/2c)\underline{\mu}'^2} F(\underline{\mu}) \delta\left(\underline{\mu}' - \underline{\mu} + \frac{\underline{x}_2}{\lambda}\right) \right. \\ & \left. e^{2\pi i \underline{\mu} \cdot \underline{\alpha}_1} d\underline{\mu} d\underline{\mu}' \right] e^{-(2\pi i/\lambda)\underline{x}_1 \cdot \underline{\alpha}_1} d\underline{\alpha}_1 \quad (74) \\ = \int e^{-(c/2)\underline{\alpha}_1^2} & \left\{ \int F(\underline{\mu}) e^{-(1/2c)[\underline{\mu} - (\underline{x}_2/\lambda)]^2} e^{2\pi i \underline{\mu} \cdot \underline{\alpha}_1} \right\} \\ & e^{-(2\pi i/\lambda)\underline{x}_1 \cdot \underline{\alpha}_1} d\underline{\alpha}_1 \quad (75) \end{aligned}$$

Changing the order of the integrations in (75) gives

$$\overline{\Gamma_o(\xi_1, \xi_2)} = \int e^{-(1/2c)[\mu - (\xi_2/\lambda)]^2} F(\mu) \left\{ \int e^{-(c/2)\alpha_1^2} e^{2\pi i \alpha_1 \cdot [\mu - (\xi_1/\lambda)]} d\alpha_1 \right\} d\mu. \quad (76)$$

The quantity in the braces is the inverse transform of (71) above, so that (76) is

$$\overline{\Gamma_o(\xi_1, \xi_2)} = \int F(\mu) e^{-(1/2c)[\mu - (\xi_2/\lambda)]^2} e^{-(1/2c)[\mu - (\xi_1/\lambda)]^2} d\mu. \quad (77)$$

The quantity  $F(\mu)$  in (77) is, according to (72), just the Fourier transform of  $e^{k^2 \phi(\alpha_1 - \alpha_2)}$ . Thus we write

$$F(\mu) = \text{F.T.} \left[ e^{k^2 \phi(\alpha_1 - \alpha_2)} \right] \\ = \text{F.T.} \left[ 1 + k^2 \phi(\alpha_1 - \alpha_2) + \frac{k^4}{2} \phi^2(\alpha_1 - \alpha_2) + \dots \right] \quad (78)$$

$$= \delta(\mu) + \text{F.T.} \left[ k^2 \phi(\alpha_1 - \alpha_2) + \frac{k^4}{2} \phi^2(\alpha_1 - \alpha_2) + \dots \right] \\ = \delta(\mu) + k^2 \tilde{\phi}(\mu) + \frac{k^4}{2} \tilde{\phi}^2(\mu) + \dots, \quad (79)$$

since the Fourier transform of a constant is the Dirac delta function. Now when (79) is substituted in (77), Eq. (77) becomes

$$\overline{\Gamma_o(\xi_1, \xi_2)} = \int \left[ \delta(\mu) + k^2 \tilde{\phi}(\mu) + \frac{k^4}{2} \phi^2(\mu) + \dots \right] e^{-(1/2c)[\mu - (\xi_2/\lambda)]^2} e^{-(1/2c)[\mu - (\xi_1/\lambda)]^2} d\mu. \quad (80)$$

The first term of (80) is the integration over the  $\delta$  function; thus we have

$$\overline{\Gamma_o(\xi_1, \xi_2)} = e^{-\frac{1}{2c\lambda^2}\xi_1^2} e^{-\frac{1}{2c\lambda^2}\xi_2^2} + \int \left[ k^2 \tilde{\phi}(\mu) + \frac{k^4}{2} \tilde{\phi}^2(\mu) + \dots \right] e^{-\frac{1}{2c}[\mu - (\xi_2/\lambda)]^2} e^{-\frac{1}{2c}[(\xi_1/\lambda)]^2} d\mu \quad (81)$$

The first term of (81) is of the form (68), which is a product of two wave amplitudes, showing that it is the coherent contribution to the ensemble-averaged mutual intensity distribution in the object plane.

To evaluate the integral term in (81), we require that  $\tilde{\phi}(\mu)$  be slowly varying over the region of the  $\mu$  plane where the integrand is non-zero. Since  $\tilde{\phi}(\mu)$  is the Fourier transform of the autocorrelation function of the glass thickness and the terms  $e^{-\frac{1}{2c}[\mu - (\xi_2/\lambda)]^2}$  are the Fourier transforms of the light amplitude distribution at the glass, this requirement corresponds physically to the requirement that the correlation interval of the glass thickness be small compared with the size of the illuminated area on the glass. Then the quantity in brackets may be taken as approximately constant, giving

$$\overline{\Gamma_o(\xi_1, \xi_2)} = e^{-\frac{1}{2c\lambda^2}\xi_1^2} e^{-\frac{1}{2c\lambda^2}\xi_2^2} + \left[ k^2 \tilde{\phi}(\mu) + \frac{k^4}{2} \tilde{\phi}^2(\mu) + \dots \right] \int e^{-\frac{1}{2c}[\mu - (\xi_2/\lambda)]^2} e^{-\frac{1}{2c}[(\xi_1/\lambda)]^2} d\mu \quad (82)$$

By making a change of variables  $\mu - \xi_2 = \mu'$ , the integral in Eq. (82) can be seen to be simply a convolution of two Gaussian functions, and the convolution of two Gaussians can be easily shown to be a Gaussian. Therefore, when (82) is evaluated it has the form

$$\overline{\Gamma_o(\xi_1, \xi_2)} = e^{-\frac{1}{2c\lambda^2}\xi_1^2} e^{-\frac{1}{2c\lambda^2}\xi_2^2} + \left[ k^2 \tilde{\phi}(\mu) + \frac{k^4}{2} \tilde{\phi}^2(\mu) + \dots \right] e^{-\frac{1}{2c\lambda^2}(\xi_1 - \xi_2)^2} \quad (83)$$

It is now apparent that the second term in (83) has the form of Eq. (9), i.e. since we assumed that  $\tilde{\phi}(\underline{\mu})$  is approximately constant, it is a function of the coordinate differences  $\underline{x}_1 - \underline{x}_2$  only and is therefore the mutual intensity that one would expect from a distant incoherent source.

It is clear that the incoherent contribution will dominate the coherent contribution when

$$k^2 \phi(\underline{\alpha}_1 - \underline{\alpha}_2) \gg 1. \quad (84)$$

To clarify the meaning of (84) we consider the region about  $\underline{\alpha}_1 - \underline{\alpha}_2 = 0$ . Since we assumed earlier that the glass thickness is a random variable with zero mean, we find that  $\phi(0) = \text{the variance } \sigma^2$ . Then (84) will become

$$\frac{(2\pi)^2 \sigma^2}{\lambda^2} \gg 1 \quad (85)$$

or

$$\sigma \gg \frac{\lambda}{2\pi}. \quad (86)$$

Thus, when the standard deviation of the glass thickness is greater than the order of a wavelength, the coherent term in (83) will be negligible. We may interpret (86) in the following way: When  $\sigma$  is greater than  $\lambda/2\pi$ , the phase of the scattered light at a point just after passing through the ground glass can be anywhere between 0 and  $2\pi$ , and the source can be expected to act as an incoherent one.

We conclude, then, that when the correlation interval of the ground glass thickness is small compared with the size of the illuminated glass area, and the standard deviation of the thickness is greater than the order of a wavelength, the ensemble-averaged mutual intensity distribution in the object plane has the same form as that we would obtain from an incoherent source. As we shall see, measurements of the mutual intensity in the object plane, taking into account the exact size of the Gaussian intensity distribution shown in Figure 6, verify this prediction.

## EXPERIMENTAL MEASUREMENTS

The experimental arrangement shown in Figure 7 was used to measure the time-averaged mutual intensity distribution in the object plane. Basically, this is a  interference experiment in which the modulus of the complex degree of coherence defined by Eq. (3) is obtained from measurements of the visibility of a fringe pattern. This pattern is produced by the interference of the light from two pinholes in an otherwise opaque screen placed in the object plane. The visibility of the fringes was first interpreted by Zernike in 1938 as a measure of the degree of coherence between these two points. (For theoretical and experimental background, see Thompson and Wolf,<sup>6</sup> and Chap. 1 of Beran and Parrent.<sup>3</sup>)

In our experiment, the radius of the pinholes was  $25\ \mu$  and their centers were separated by  $500\ \mu$ . A lens of focal length  $f_2 = 50\ \text{mm}$ , shown in Figure 7, was placed to the right of the object plane so that the interference pattern produced by the two pinholes appeared in an observation plane one focal length to the right of the lens. The auxiliary lens just to the left of the ground glass was used to adjust the size of the illuminated area on the ground glass.

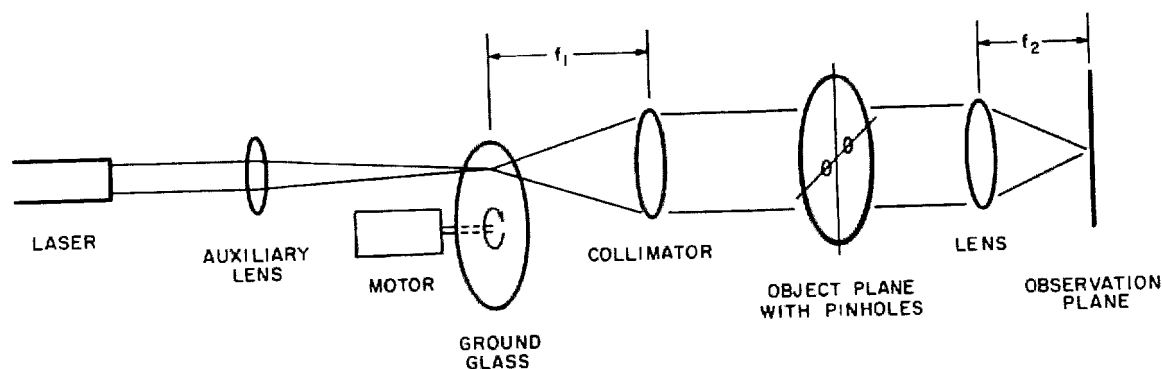


Figure 7. Experimental Arrangement for Measuring Degree of Coherence

When the laser is operated with a hemispherical cavity in the lowest order mode, the intensity across the beam is essentially Gaussian in shape. (Measured values were compared with a Gaussian in Figure 6.) Since the aperture of the auxiliary lens is considerably larger than the characteristic width of the laser beam, the aperture effect of the lens can be neglected and the intensity across the beam when it is incident on the ground glass remains Gaussian.

If the rotating ground glass acts as an incoherent source in the time average, then according to the van Cittert-Zernike theorem expressed by Eq. (9), the mutual intensity distribution in the object plane is the Fourier transform of the intensity distribution on the ground glass and is a function of coordinate differences only. Thus using the normalized form of (9) defined by (3), we should obtain

$$\gamma(\xi_1, \xi_2) = \gamma(\xi_1 - \xi_2) = \frac{\int_{-\infty}^{\infty} I(\underline{\alpha}) e^{(2\pi i / \lambda f_1) \underline{\alpha} \cdot (\xi_1 - \xi_2)} d\underline{\alpha}}{\int_{-\infty}^{\infty} I(\underline{\alpha}) d\underline{\alpha}}, \quad (87)$$

where

$\xi$  = coordinate in object plane

$\underline{\alpha}$  = coordinate in plane of ground glass

$\gamma(\xi_1, \xi_2)$  = complex degree of coherence

$I(\underline{\alpha})$  = intensity distribution on ground glass

$f_1$  = focal length of collimator lens = 26 in.

$\lambda$  = wavelength of laser light = 6328 Å.

The particular scale of  $\gamma(\xi_1 - \xi_2)$  can be found by using the form of  $I(\underline{\alpha})$  shown by Figure 6:

$$I(\underline{\alpha}) = e^{-\underline{\alpha}^2 / s^2}, \quad (88)$$

where  $s$  = the  $1/e$  point. (Figure 6 shows the particular case of  $s = 0.8$  mm.) Using the form of (88) in (87) gives

$$\gamma(\xi_1 - \xi_2) = e^{-\left[ \pi^2 s^2 / \left( \lambda^2 f_1^2 \right) \right] (\xi_1 - \xi_2)^2}, \quad (89)$$



since the Fourier transform of a Gaussian is a Gaussian. Experimentally, it was found more convenient to vary the size  $s$  of the source rather than change the separation of the pinholes  $(\xi_1 - \xi_2)$ . The two techniques are equivalent as can be seen from an examination of (89). The modulus of  $\gamma(\xi_1 - \xi_2)$  is shown in Chap. 1 of Beran and Parrent<sup>3</sup> to be identical with the visibility of the fringes obtained in the observation plane. For the Gaussian, we have  $\gamma(\xi_1 - \xi_2) = |\gamma(\xi_1 - \xi_2)|$ .

Figure 8 shows the measured  $|\gamma(\xi_1 - \xi_2)| = |\gamma_{12}|$  compared with the predicted values given by (89). The ranges in the experimental values result from possible inaccuracies in determining the focal length of the auxiliary lens and an approximate 2 mm wobble in the ground glass as it rotates.

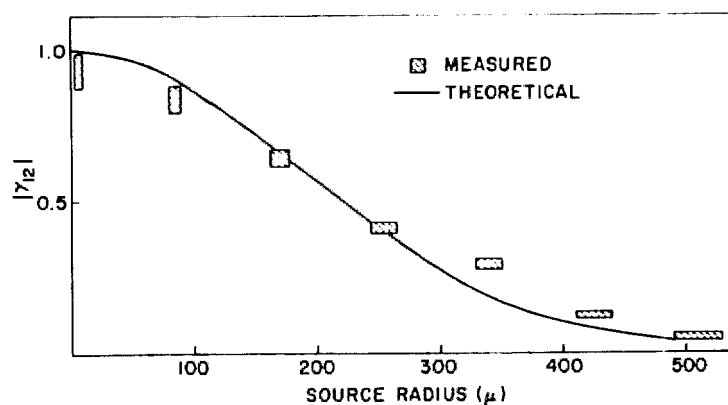


Figure 8. Theoretical and Experimental Values of  $|\gamma_{12}|$  vs Source Radius

Measurements made for various locations of the pinholes in the object plane (always maintaining their 500  $\mu$  separation) produced results that are essentially identical with those shown in Figure 8. Some of the fringe patterns and their corresponding microdensitometer traces from which the visibility was determined are shown in Figure 9. To determine the actual visibility, one must go through the D log E curve and compensate for any modulation loss in the film. However, SO-243 film was used to record the interference patterns; the separation of the fringe maxima was approximately 60  $\mu$ , so that film losses and microdensitometer transfer function effects were negligible.

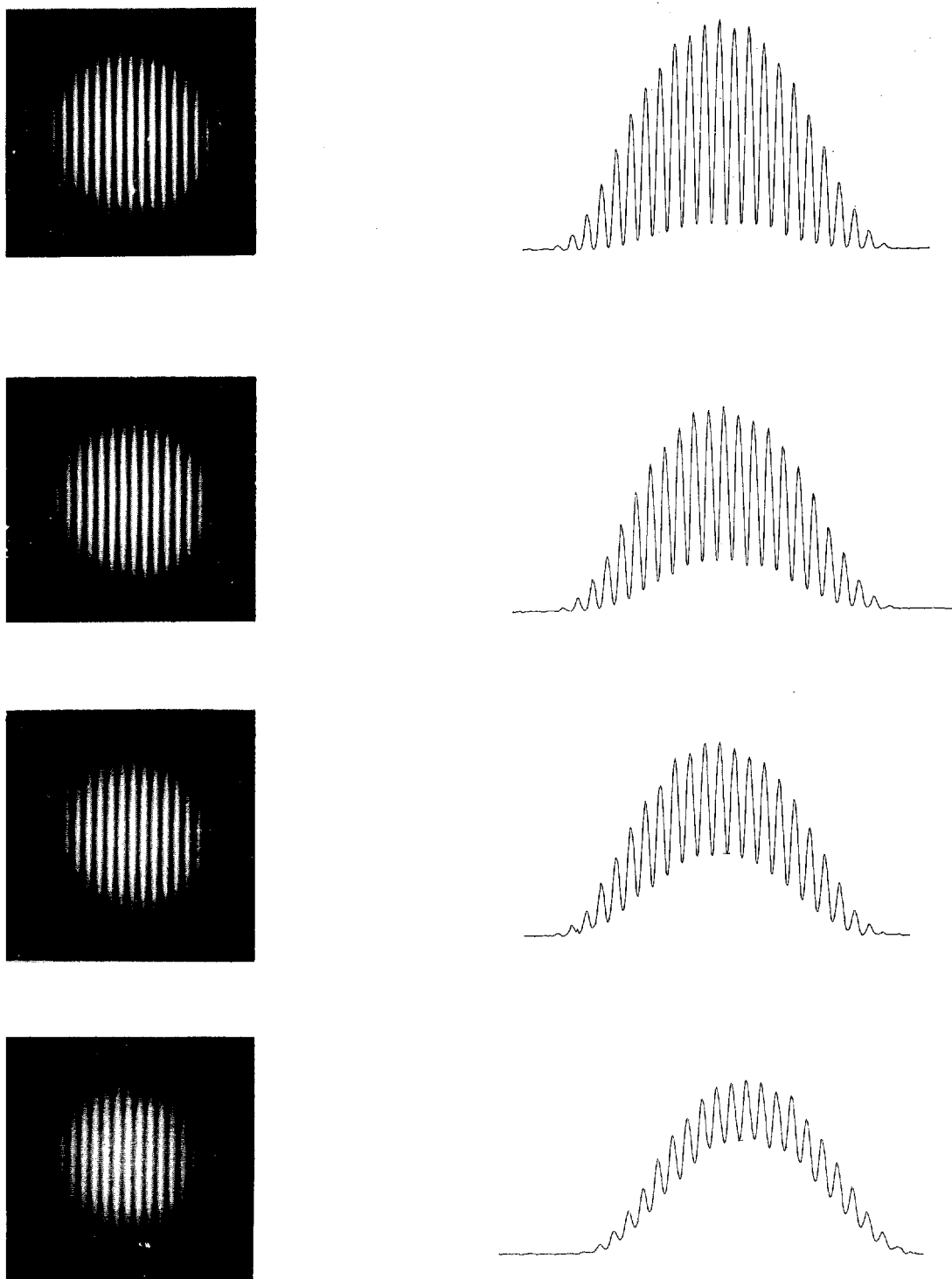


Figure 9. Fringe Patterns (at 25X Magnification) from Two-Pinhole Interferometer and Their Corresponding Microdensitometer Traces

The results show excellent agreement with the mutual intensity distribution expected from an application of the van Cittert-Zernike theorem and the assumption of an incoherent source, and also with the form expected from the theoretical considerations presented in the first part of this chapter.

The measurements described above were made for the laser operating in its lowest order mode. To provide the maximum power, the laser is often operated in higher order modes. Because it is difficult to characterize the intensity distribution on the ground glass for these higher order modes, quantitative predictions of  $\gamma(\xi_1, \xi_2)$  were not made. However, measurements indicated that when the illuminated area of the ground glass was approximately the same as in the lowest order mode case,  $\gamma(\xi_1 - \xi_2)$  was only slightly lower than the distribution for the lowest order mode shown in Figure 8.




## CHAPTER 4

### INCOHERENT TRANSFER FUNCTION MEASUREMENTS

In the theoretical calculations of partially coherent images, the imaging system is assumed to be free of aberrations for on-axis imagery. To test the validity of this assumption, and to obtain a quantitative measure of system quality, measurements of the incoherent modulation transfer function of the enlarger were made. Since the object plane illumination is partially coherent when the enlarger is used as designed, a piece of ground glass must be moved rapidly up and down directly in front of the object plane to produce incoherent illumination effectively.

The primary method used for these measurements was an edge imaging process. Results were checked by comparing them with images of the 15-cycle square-wave target run through the enlarger (for a description of this target see Chap. 5, p. 55).

The edge imaging process consisted of the following steps:

1. An edge of 3.5:1 contrast was incoherently imaged through the system and the film was processed with sensitometric control.
2. The edge image was traced with the  microdensitometer and the densities were converted to intensities through the D log E curve.
3. The intensity distribution in the edge was differentiated by the computer to give the impulse response of the system.
4. The Fourier transform of the impulse response, which is the transfer function of the system, was found by computer.

25X1

Several assumptions are inherent in this process. It must be assumed that the edge object contains perfect spatial frequency information throughout the required range, which extends to about 400  $\ell$ /mm. For practical purposes, a good razor blade edge would probably be a sharp enough object, but it would provide infinite contrast and require prefogging of the film. The actual edge used, supplied

25X1

25X1

[ ] is of 3.5:1 contrast and is composed of chromium deposited on a glass substrate. Photomicrographs of this edge and also a razor edge are shown in Figure 10. Variations in the razor edge are of the order of  $1\ \mu$ , those in the [ ] edge are considerably less in selected areas.

25X1

Another assumption in this process is that the microdensitometer does not affect the measurement in any unknown way. Since the spatial frequencies in the image range only to about  $100\ \ell/\text{mm}$  (a result of the 4X magnification), the microdensitometer is used well within its resolution limit, and it is safe to assume that the effect of the microdensitometer can be represented by the modulation transfer function of its scanning slit. The scanning slit used was  $5\ \mu$  in width, and the effect of its transfer function was accounted for in analyzing the edge traces.

The chief drawback of the edge trace analysis is that a large amount of information is obtained from a small sample, and the result is extremely sensitive to any microscopic effects in the film. A problem often encountered in such work is grain noise in the trace; when this occurs, it must be filtered out to obtain optimum results. Since the resolution limit of the film is much greater than that of the overall system, in our work the microdensitometer slit could be made sufficiently wide to eliminate grain noise without affecting the resolution of the trace.

Figure 11 shows the result obtained for the modulation transfer function of the system for incoherent illumination at  $6328\ \text{\AA}$ . This result is the average of four measurements made on edges that were exposed and processed separately. The averaging process helps to compensate for the small samples used in the individual measurements. Each exposure analyzed was the best focused exposure from a through-focus run.

To find the lens transfer function from these data, it is necessary to correct for the film transfer function — a function of contrast, exposure, and development. Ideally, this function should be known under the exact conditions used in these experiments. However, since the shape of the system transfer function is dominated by the lens transfer function and the film transfer function provides only a small correction, the film transfer function need not be known precisely to provide the necessary correction. Therefore, we used the transfer function for this film

25X1

Approved For Release 2002/07/12 : CIA-RDP78B04747A002700020022-7  
ILLEGIB

Approved For Release 2002/07/12 : CIA-RDP78B04747A002700020022-7

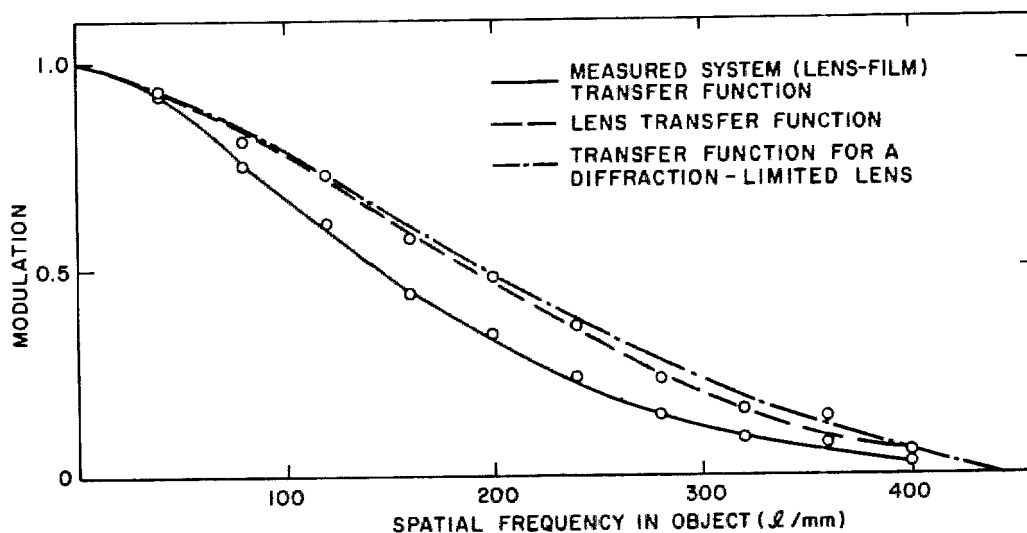


Figure 11. Transfer Function for Incoherent Illumination at 6328 Å

Figure 11 also shows the resulting lens transfer function compared with the theoretical diffraction-limited transfer function. The agreement is quite good, although the experimental result does not quite achieve the ideal curve. We conclude, however, that for practical purposes the lens system can be considered to be diffraction-limited on axis.

To obtain some sort of check on this result, measurements were made of the contrast reduction resulting from imaging a high-contrast 15-cycle square-wave target through the system. This target had a maximum frequency of 1000 l/mm and was essentially of infinite contrast. Since this target resembles a pure square wave near the center of one of the 15-cycle groups, its design enables the measurement of the cutoff frequency of a lens. Beyond half the cutoff frequency, the system passes only the fundamental frequency of the square wave, which of course is a sine wave of the same frequency. The modulation reduction measurements in this region are thus equivalent to transfer function measurements.

Figure 12 shows the results of this measurement. Beyond 200 l/mm, the curve is fairly close to that for the edge measurements. Below 200 l/mm, the modulation for the square-wave target is higher. This is expected, of course, because frequencies higher than the fundamental one are also passed, resulting in higher contrast images.

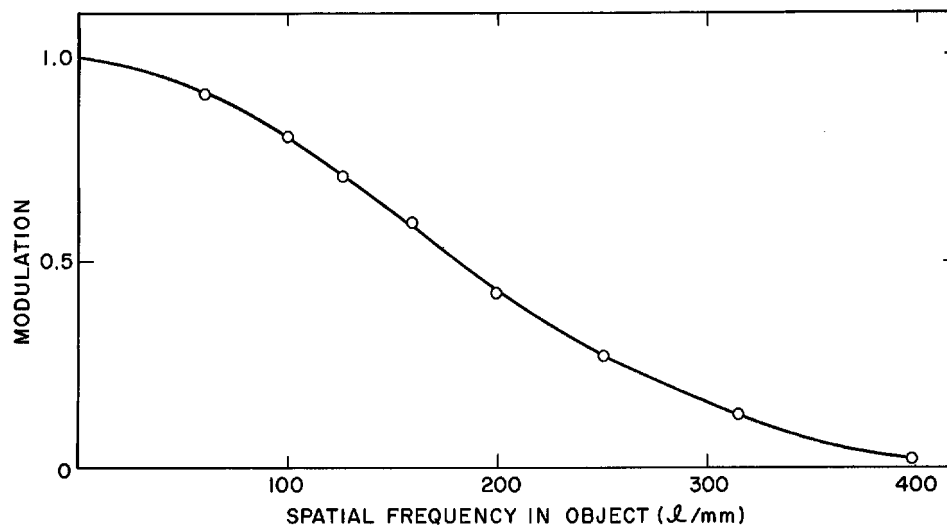


Figure 12. Modulation of Square Wave Target for Incoherent Illumination at 6328 Å

Measurements were also made of the transfer function for incoherent sodium illumination. Again, the incoherent illumination was obtained by moving a piece of ground glass up and down directly in front of the object plane. Measurements on the square wave target indicated that the transfer function was essentially equivalent to that for the incoherent laser illumination. Because of the shorter wavelength of the sodium source, however, the transfer function for a diffraction-limited lens should be slightly better. Thus, the imaging system for the sodium wavelength is not as close to diffraction-limited as it is for the laser wavelength.

Measurements of transfer functions were made as the edge was moved through focus in the object plane. The depth of focus in the image was sixteen times that in the object because of the 4X magnification used. Results of a particular through-focus run made with the sodium source are plotted in Figure 13. When the edge was  $\pm 0.0007$  in. out of focus degradation was noticeable, and when it was  $\pm 0.0015$  in. out of focus degradation was rather severe. Experience has shown that the first lens can be reproducibly set to within  $\pm 0.0002$  in. and the second lens to within  $\pm 0.002$  in. The defocusing effect from moving the second lens by this amount was approximately the same as that produced by a  $\pm 0.0001$  in. movement of the first



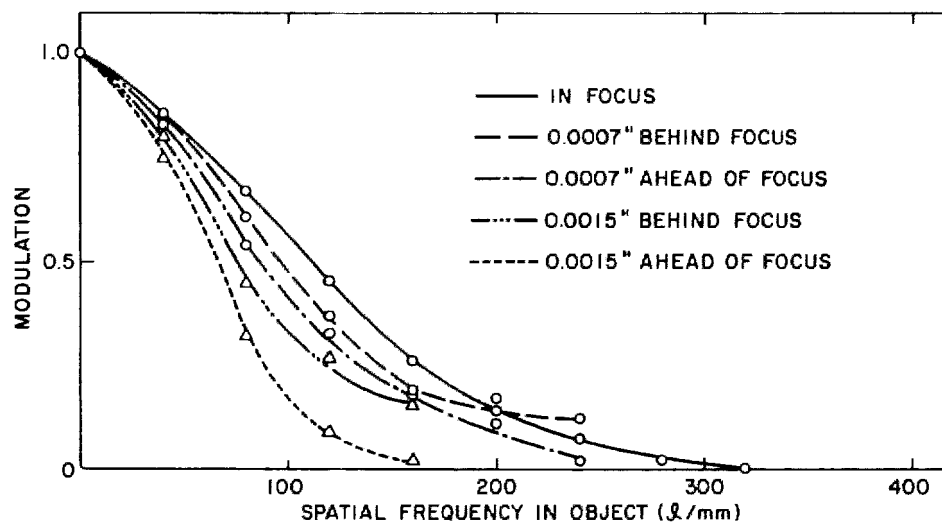


Figure 13. Modulation Transfer Functions for Various Positions in a Through-Focus Test

lens. Overall reproducibility was thus about  $\pm 0.0003$  in. at the object, and we can infer from the results in Figure 13 that this caused negligible image degradation. Images made of resolution targets throughout the course of this work indicated that there was no problem in obtaining the required focal reproducibility.

## CHAPTER 5

### IMAGING STUDIES

We showed in Chap. 2 that the image intensity distribution in a partially coherent imaging system depends on the three factors exhibited in Eq. (16). Having determined the first two of these — the coherence of the object illumination (Chap. 3) and the amplitude impulse response (Chap. 4) — we now specify the third factor and thereby apply the theory to the imaging of specific objects. Since we are dealing with a nonlinear imaging situation, it is impossible to predict from simple objects how the more complex ones will be imaged. Therefore, to gain experience with the imaging problem, we imaged progressively more complex objects, predicting the image intensity distribution for the less complex cases as a test of the theory and of the results obtained in Chaps. 3 and 4.

The important parameter in partially coherent imaging employing primary incoherent sources was found (Chap. 2) to be the relative scale of the mutual intensity function and the impulse response. The particular case considered in Chap. 2 was, for the sake of simplicity, the unit magnification system.

It should be noted that this relative scale characterizes the imaging situation only when the primary source is incoherent, i.e. only when the mutual intensity distribution in the object plane is a function of coordinate difference. This characterization therefore depends on the results presented in Chap. 3, where the illuminated rotating ground glass disc is shown to be an effectively incoherent source.

The forms found for the impulse response and object plane mutual intensity function are illustrated in Figure 14. The ratio  $D$ , which we define as

$$D = \frac{\alpha}{\beta}, \quad (90)$$

is the ratio of the widths at the 0.88 points (shown by the arrows in Figure 14) and it decreases as the system becomes more coherent.

An "apparent" transfer function defined as in Chap. 2 was calculated for each of the theoretical edge images. Although it serves as a description of the effect of coherence on the spatial frequency content of these particular objects, it should not,

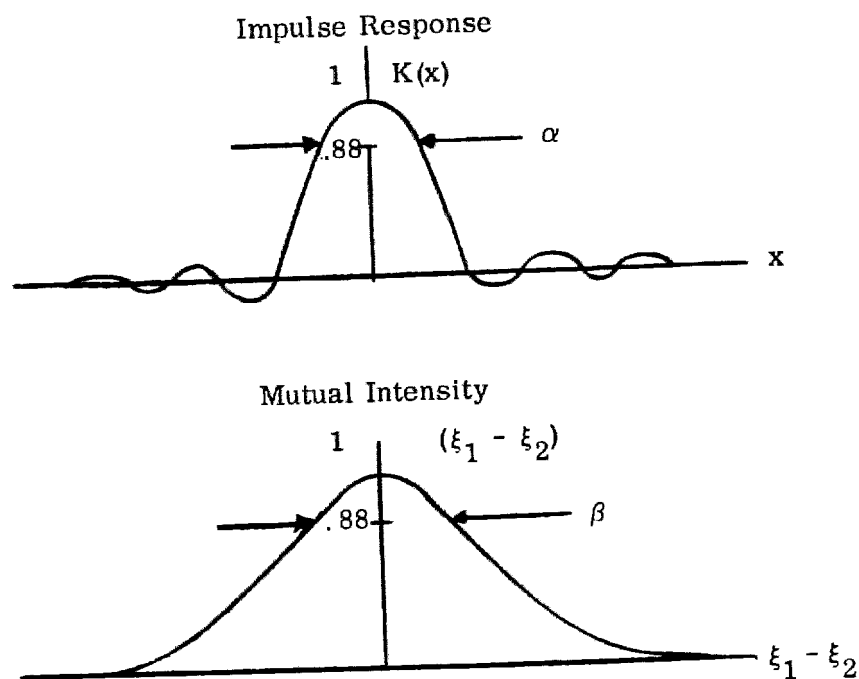


Figure 14. Impulse Response of System and Object Plane Mutual Intensity Function

as pointed out in Chap. 2, be interpreted as a valid transfer function. The consequences of such a misinterpretation are graphically illustrated later in Chap. 7.

## THEORETICAL AND EXPERIMENTAL

### EDGE IMAGES

Both experimental measurements and theoretical calculations of the 3.5:1 contrast Mann edge were made at various coherence intervals in the object plane. The theoretical calculations for the Gaussian coherence function characteristic of the laser illumination in the instrument indicated that the calculated edges were identical for values of  $D$  less than  $1/8$ , indicating that in this particular experiment the coherent limit was reached when  $D \approx 1/8$ . Slight differences occurred in the calculated values of  $D$  between  $1/2$  and  $1/8$ , but for practical purposes the images were identical. Although noticeable differences occurred for  $D = 1$  as compared with the values given above, pronounced ringing was still evident. Several of these calculated results are reproduced in Figure 15, and the corresponding apparent transfer functions are shown in Figure 16.

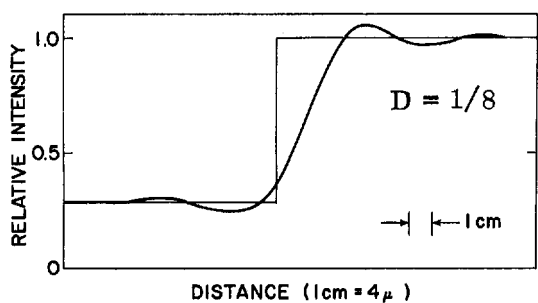
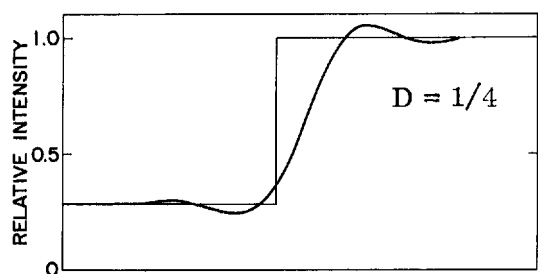
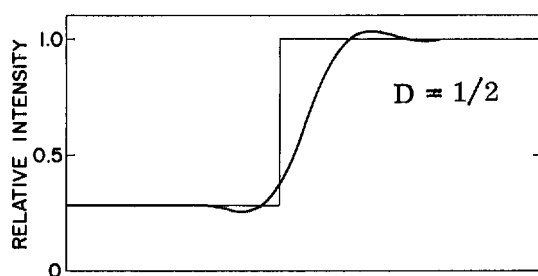
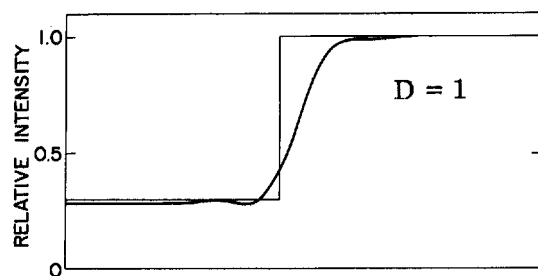


Figure 15. Calculated Edge Images for Various Values of D

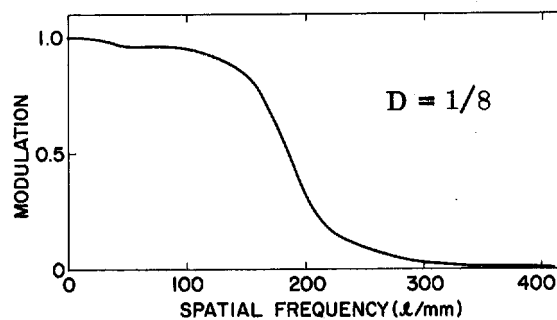
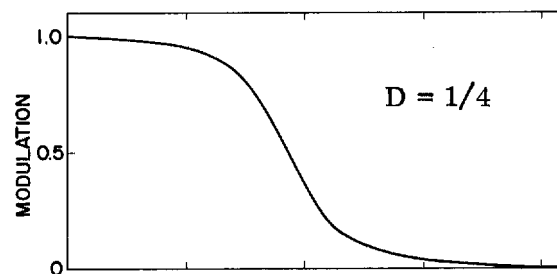
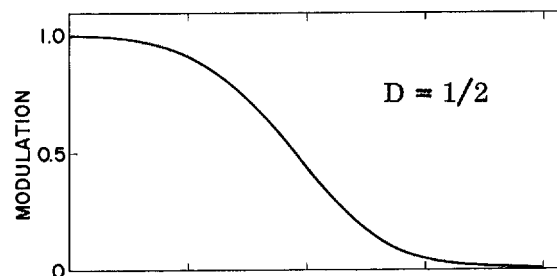
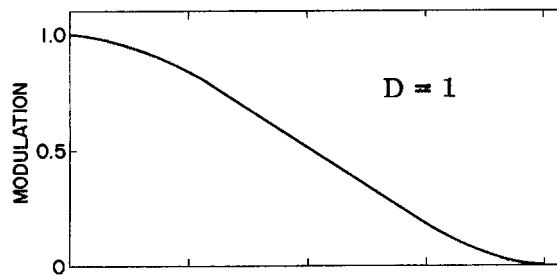


Figure 16. Apparent Transfer Functions for the Edge Images of Figure 15

As previously noted, the smallest coherence interval using the laser source was  $25 \mu$ ; this occurred when the multimode laser beam was allowed to strike the rotating diffuser unfocused. The spot size of the imaging system was  $0.6 \mu$ , giving a D value of  $1/40$ . It was determined from the edge image calculations for various values of D that the instrument operated in the coherent limit under these conditions.

A measured edge image and the calculated image for  $D = 1/40$  are in fairly good agreement (Figure 17). The calculated image, of course, applies to the aerial image; to arrive at the measured image the aerial image must be recorded on film, the film traced with a microdensitometer, and the trace corrected for the  $D \log E$  curve. It is somewhat disturbing that the result shows the measured image to have a higher gradient than the theoretical value. This could be explained if the actual cutoff frequency of the system was greater than that used in the calculation, but there is no reason to believe this is the case. A possible explanation is that adjacency effects in the film enhanced the gradient of the recorded image.

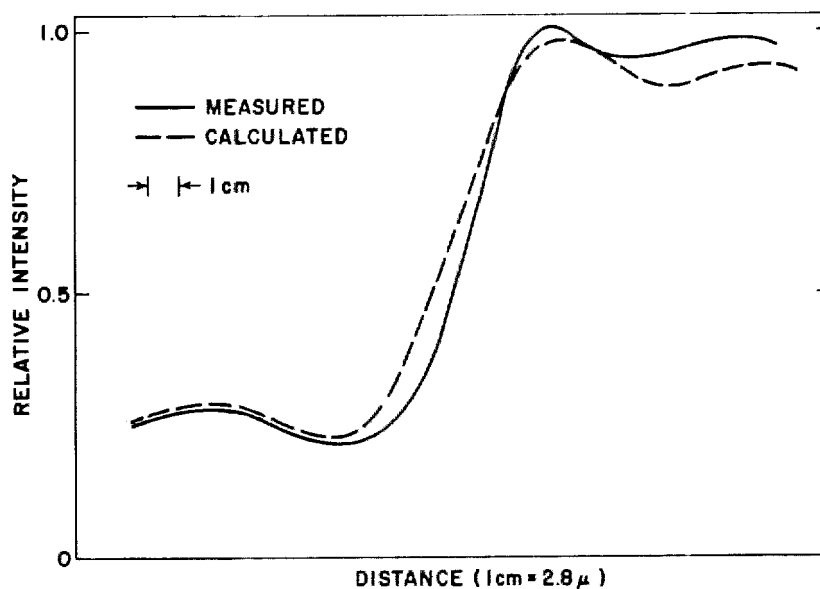


Figure 17. Measured vs Calculated Coherent Edge Images for  $D = 1/40$

Figure 18 shows an experimental incoherent image compared with the image calculated for  $D = 10$ . Although the calculated image for  $D = 10$  looks considerably

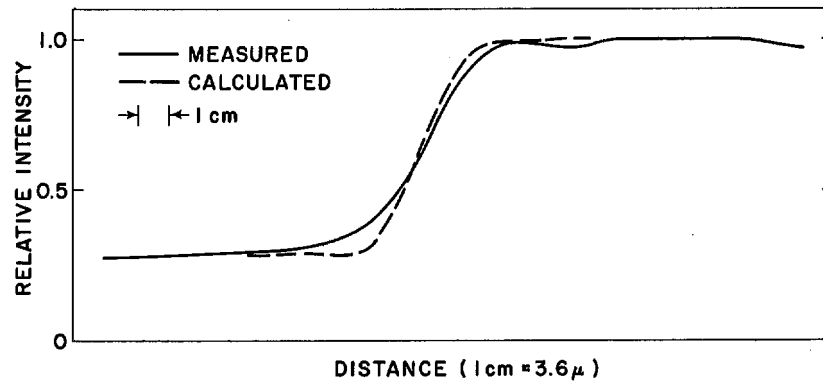


Figure 18. Measured Incoherent Edge vs Calculated Edge for  $D = 10$

less "coherent" than for the other values of  $D$  used, it appears somewhat more "coherent" than the incoherent image. This is a good indication that moving the ground glass up and down in front of the object does, essentially, make the illumination incoherent.

The most convenient way of varying the ratio of  $D$  in this instrument is to keep the coherence interval fixed at  $25 \mu$  and vary the spot size of the imaging system by changing the size of the aperture in the transform plane. To facilitate this, the fixed aperture supplied with the instrument was replaced by an adjustable iris diaphragm. The iris could be varied from 0.5 in. to 2.5 in., giving a range of  $D$  values from  $1/8$  to  $1/40$ , which enabled us to check the predicted result — that the imagery should be identical over this range.

Figure 19 shows microdensitometer traces for three different values of  $D$ . The traces are adjusted to the same scale, since changing the transform plane aperture requires that the coordinates of the trace be suitably normalized. Although the three traces have the same general characteristics, they differ slightly — particularly the  $D=1/8$  trace. There are several possible reasons for this. The change in scale produced by varying the transform plane aperture causes the film transfer function to affect the three exposures differently and may also somewhat change the aberration balance of the lenses.

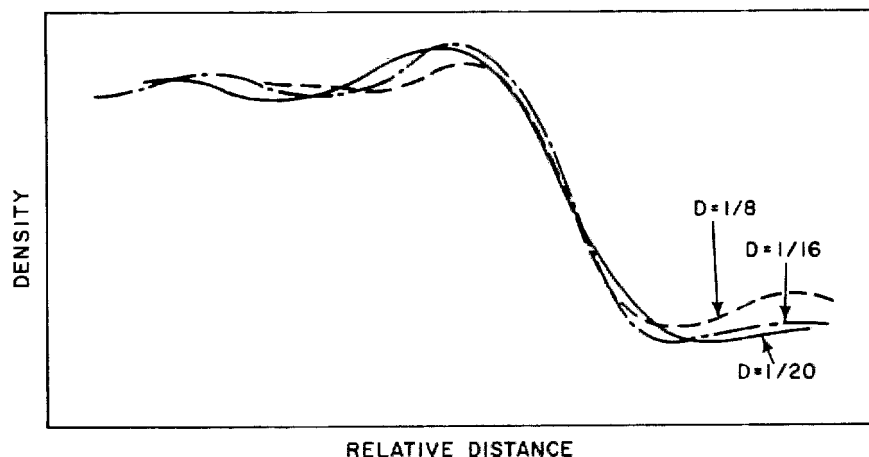


Figure 19. Microdensitometer Traces of Experimental Edge Images for Several Values of D

When a coherently illuminated high-contrast edge is imaged, the apparent position of the edge shifts. If the position of the edge is considered to be at the half-intensity point, then the shift for a one-dimensional imaging system is given by<sup>4</sup>

$$D = 0.212 (1 + m) \lambda f, \quad (91)$$

where  $m$  is the magnification and  $f$  is the  $f$ -number of the lens. To measure\* this shift, the width of a space in the low-frequency region of the 1000:1 contrast

target was measured in both coherent and incoherent images from microdensitometer traces (Figure 20). The shift in one edge is half the difference in width of the space.

The shift calculated from Eq. (91) is  $2.3 \mu$ ; the measured value is  $1.7 \mu \pm 0.4 \mu$ . The explanation for this difference in the two values is, perhaps, that the theory is for a one-dimensional imaging system and the shift is smaller than the resolving power of the film. The shift that does occur, however, is approximately equal to the expected value.

An important practical consideration is whether a photointerpreter would actually measure this shift, for he must judge the position of the edge and may well not choose the half-exposure points in both the coherent and incoherent cases.

\* For experimental measurements of the edge shift, see article by P. Considine that will appear in the August 1966 issue of J. Opt. Soc. Am.

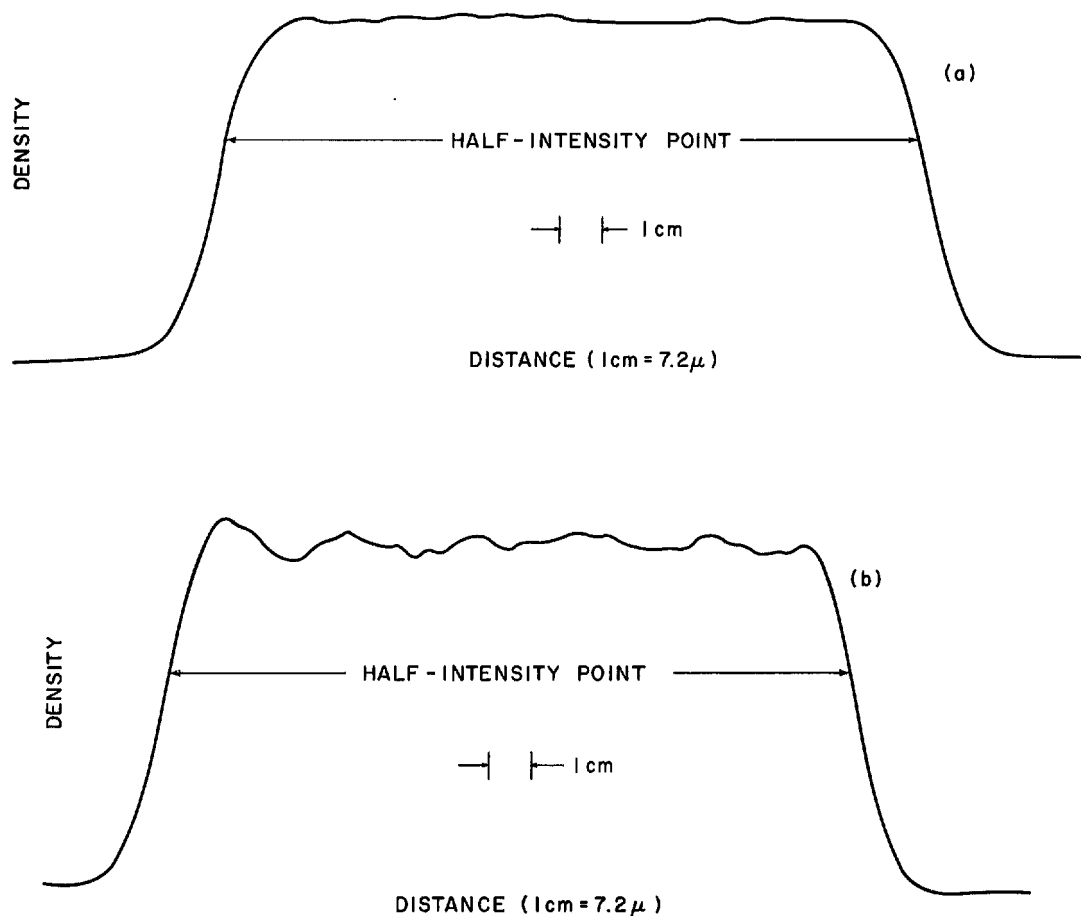


Figure 20. Microdensitometer Traces of High-Contrast Edges Showing Edge Shift for Incoherent (a) and Coherent (b) Illuminations

Measurements of the shift were also made with a Filar eyepiece and microscope. The width of the space was measured at six different positions for both the coherent and incoherent images and the results averaged. The shift in this case was  $1.1 \pm 0.8 \mu$  and was thus on the order of the accuracy of the measurement. In any case, the shift is much less than the resolution limit of the system. Whether or not this is a problem depends on the precision required in a particular case.

#### "L" TARGETS

The [ ] targets were used to obtain a comparison between experimental and theoretical images for objects more complicated than a simple edge, and



to demonstrate the nonlinearity of partially coherent imaging. Figure 21 is the high-contrast target used in this evaluation.

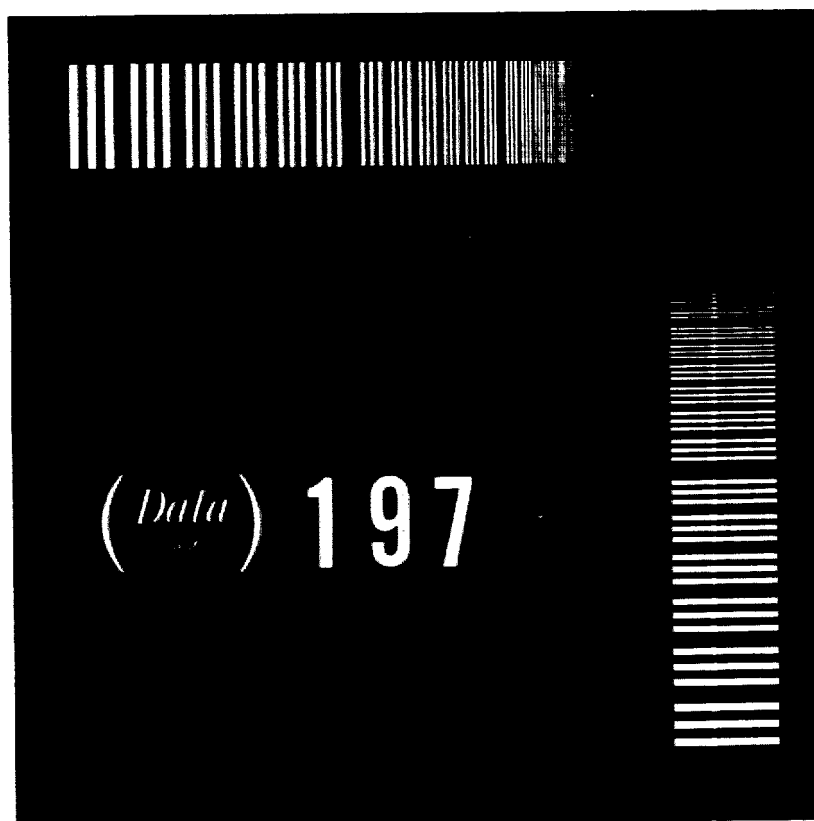


Figure 21.  "L" Target  
(10X Magnification)

Early experimental results indicated that the imagery of groups near the coherent cutoff frequency ( $225 \text{ } \ell/\text{mm}$ ) was considerably different in coherent and incoherent light. Figure 22 shows photomicrographs and microdensitometer traces of a section of the high-contrast target imaged both coherently and incoherently. When these exposures were made, the transform plane aperture was 1.25 in., resulting in a coherent cutoff frequency of about  $112 \text{ } \ell/\text{mm}$ . The dominant feature of the coherent image is where the three-bar groups imaged to two bars. Even in some of the groups that imaged as three bars, the relative heights of the bars were altered. Some fringing also occurred between groups.

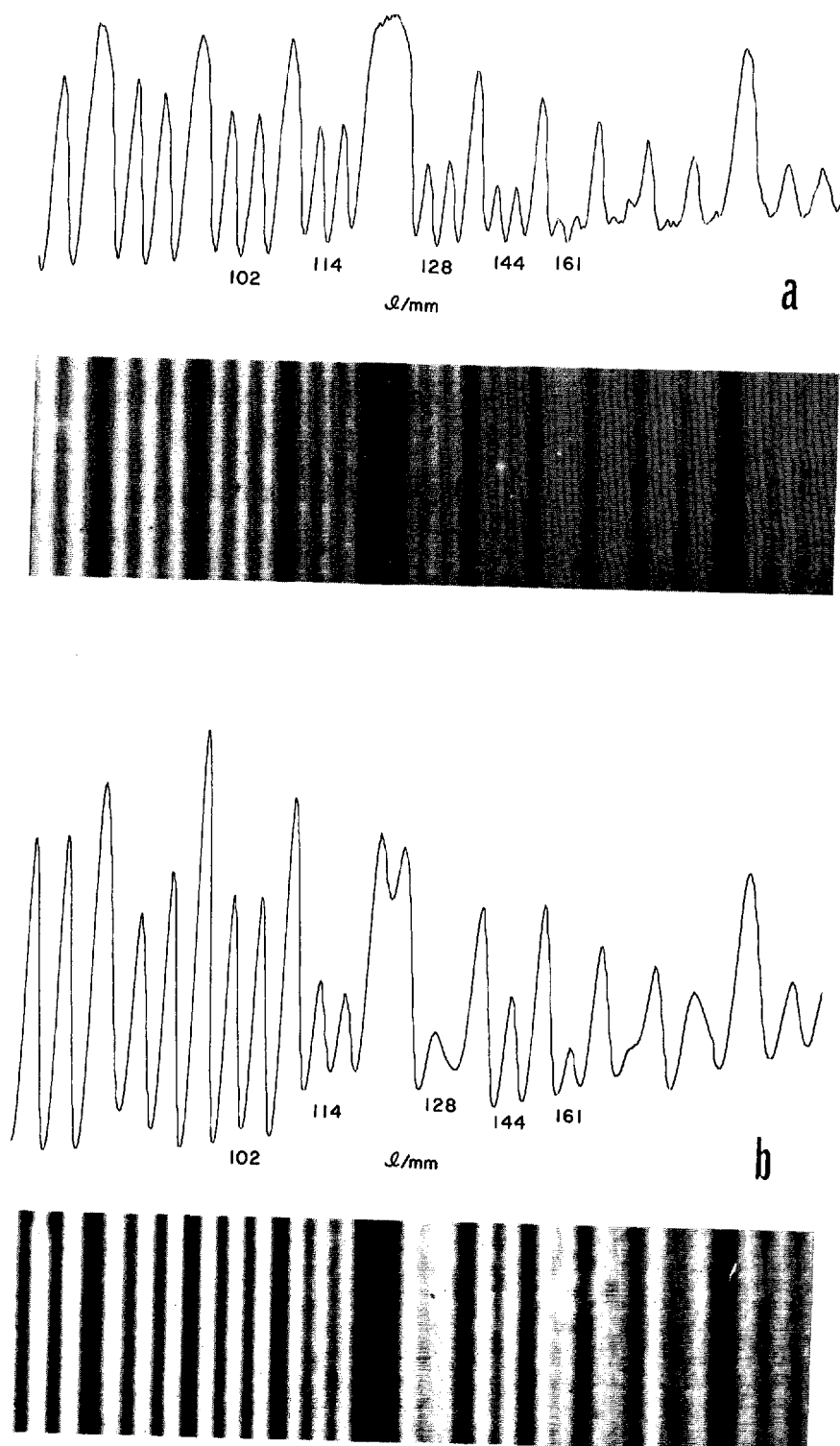


Figure 22. Photomicrographs and Microdensitometer Traces of "L" Target Coherently (a) and Incoherently (b) Imaged

Inasmuch as the most interesting effects seemed to occur near the coherent cutoff frequency, one three-bar group in each contrast target was chosen for theoretical analysis. In the calculations, the effects of two three-bar groups on each side of the group under consideration was taken into account.

For the high-contrast object, the group analyzed was at a frequency of 256  $\ell/\text{mm}$ . This was the first group where the original three bars imaged into two bars with the transform plane aperture at its normal value of 2.5 in. Figure 23 shows the experimental and theoretical results superimposed on the original. Here, again, the calculation is for the aerial image, while the experimental results involve film storage of the image and microdensitometer analysis. In addition, the object may not be a perfectly square three-bar group, as is assumed in the calculation.

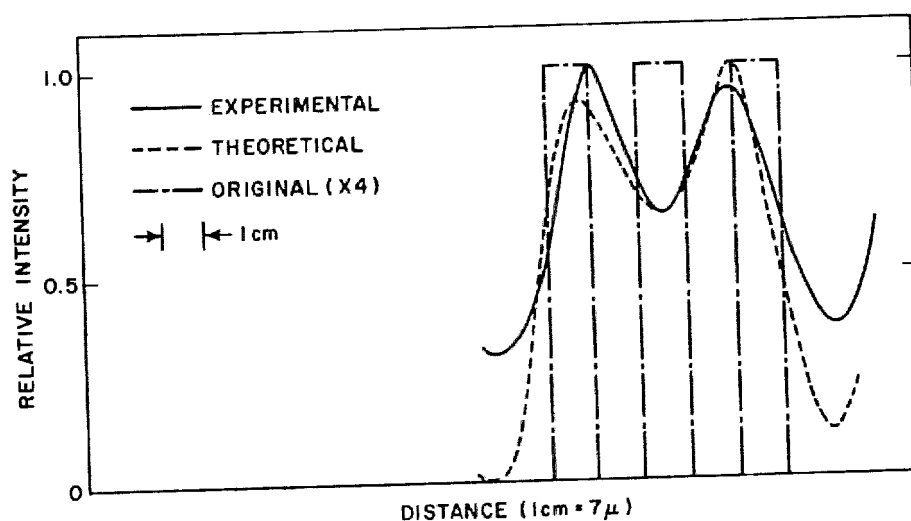


Figure 23. Image of 256  $\ell/\text{mm}$  Group in High-Contrast "L" Target vs Calculated Image. (Peak intensities in the images are not normalized with respect to the original object.)

For the low-contrast target, a group at 203  $\ell/\text{mm}$  was analyzed. This group imaged as three bars, but with a variation in the height of the peaks. The measured image exhibited considerably lower modulation than predicted. The object at this frequency had a much lower contrast than the nominal 2:1 contrast of the target, apparently because of the modulation of the film on which the target was

formed. The calculation, however, could also be applied to the target at  $102 \ell/\text{mm}$  if the transform plane was stopped down to half its normal value. The result thus obtained is shown in Figure 24 in comparison with the theoretical result. In both cases, the height of the peaks increases towards the left, although this effect is not as strong in the measured as in the calculated image. Again, this may result from the aerial image's being obtained by analysis of the film image rather than by direct measurement.

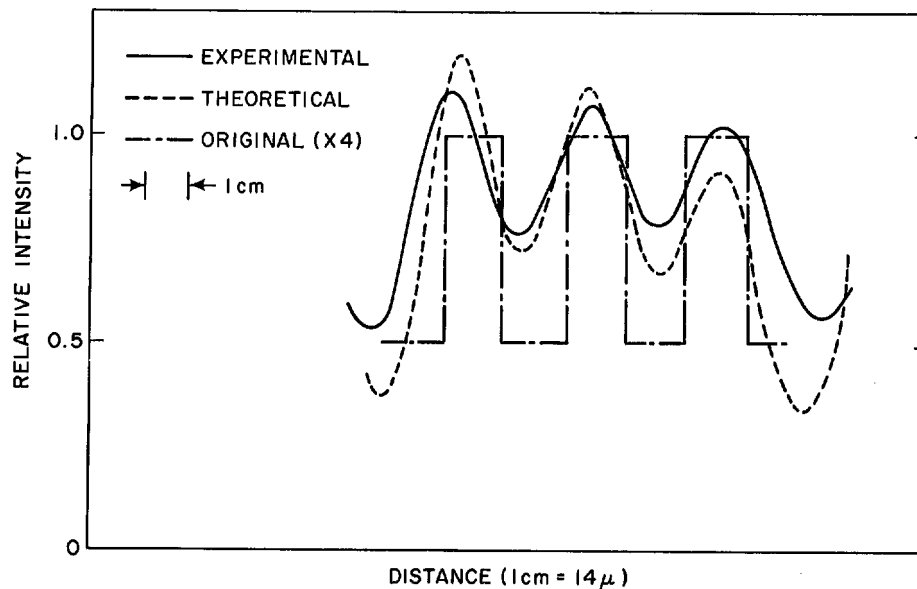


Figure 24. Measured Image of Low-Contrast Three-Bar Group at  $102 \ell/\text{mm}$  vs Calculated Result. (Peak intensities in the images are not normalized with respect to the original object.)

As with the edges, there was no difference in the calculated images for values of  $D \leq 1/8$ . Images were made for various values of  $D$  in this coherent limit by again keeping the coherence interval fixed at  $25 \mu$  and varying the transform plane aperture. The microdensitometer traces of images of the high-contrast target shown in Figure 25 were made with arms of different ratios varying directly relative to the transform plane diameters. This procedure scales the coordinates appropriately, so that the traces are on the same scale. Theory predicts that all three traces should be identical; they are, in fact, essentially similar. The differences that do exist can be attributed to possible variations in the aberration balance

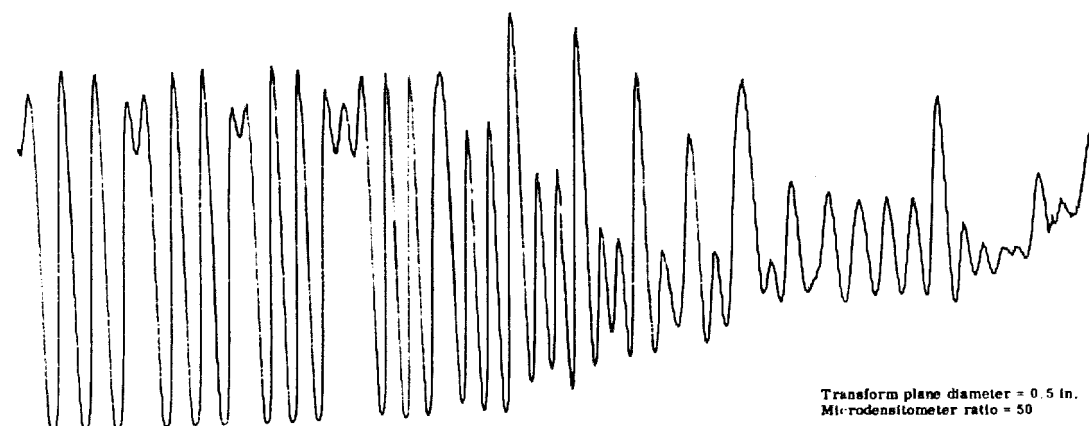
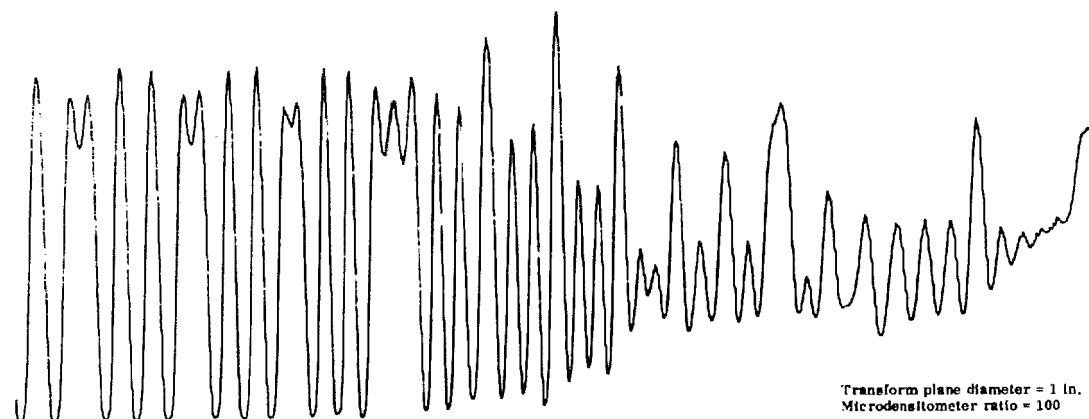
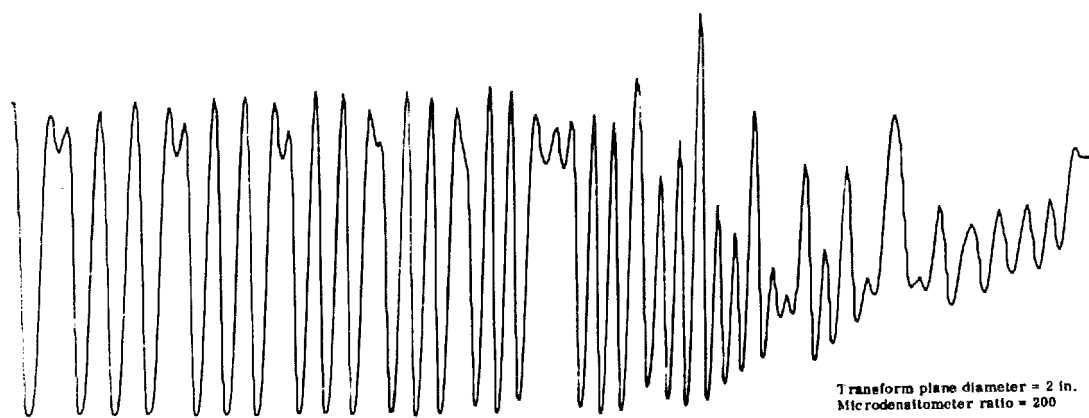


Figure 25. Microdensitometer Traces of High-Contrast "L" Target for Three Different Values of Transform Aperture Size

as the system stopped down, and to the fact that different areas of the object produced corresponding parts of these traces.

## EXPERIMENTAL

### USAF THREE-BAR TARGETS

To study imagery over the entire 9 in. image format, a target consisting of an array of nine USAF resolution targets with maximum frequencies of 228  $\ell$ /mm was used. These were arranged with one target in the center, four others  $3/4$  in. from the center, and the remaining four in the corners, forming a square with 2 in. sides.

Figures 26 and 27 are photomicrographs of the central portions of eight of the targets. One of the corner images was blocked out by an auxiliary optical system that imaged exposure data in that corner of the film. For the incoherent images there was little deterioration in the four inner targets as compared with the central target; there was considerable deterioration in the outer targets however. The coherent images again exhibited some undesirable effects, particularly at the higher frequencies.

### SQUARE-WAVE TARGET

The square-wave target used in the incoherent transfer function measurements was also imaged under various conditions of coherence. Photomicrographs of images of this target are shown in Figure 28. In these pictures, the cutoff frequency appears to decrease as the coherence interval increases. For frequencies below cutoff, the partially coherent images show higher contrast than does the incoherent image. Also the partially coherent images show some spurious detail.

25X1

Approved For Release 2002/07/12 : CIA-RDP78B04747A002700020022-7

25X1

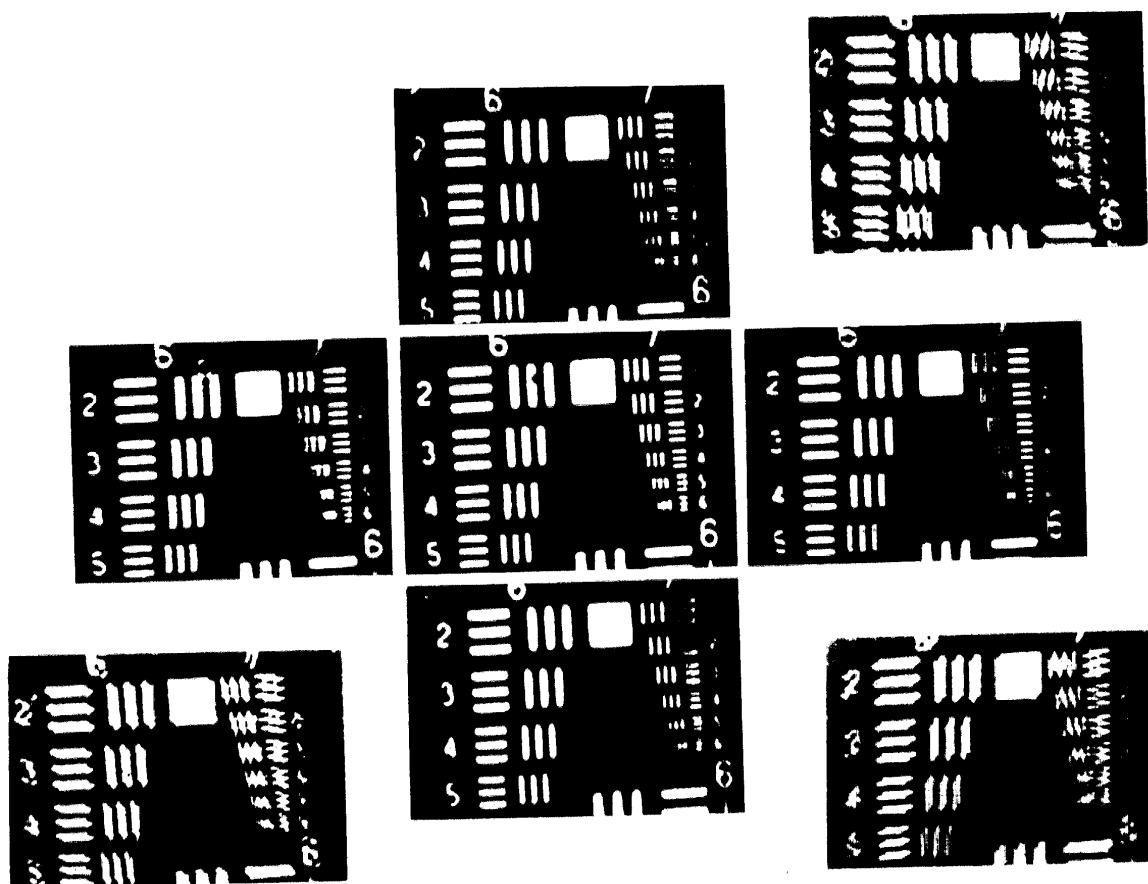


Figure 26. Photomicrographs of Coherent Images of Three-Bar Targets Over Entire Format  
(2200X Magnification over original object)

Approved For Release 2002/07/12 : CIA-RDP78B04747A002700020022-7

25X1

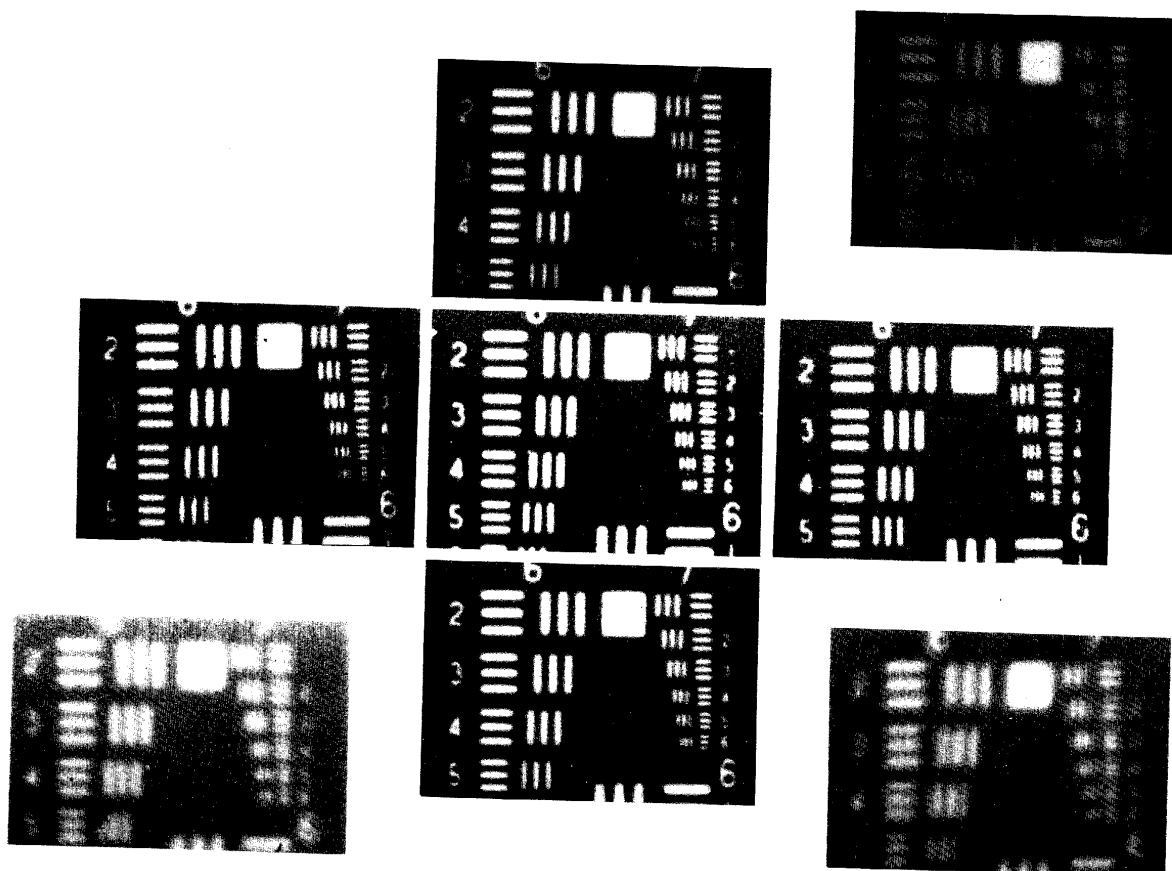
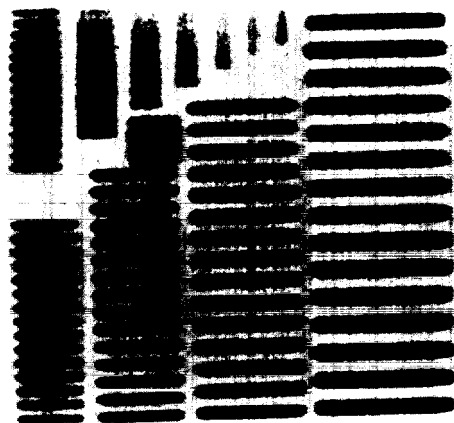


Figure 27. Photomicrographs of Incoherent Images of Three-Bar Targets Over Entire Format (2200X Magnification over original object)

25X1

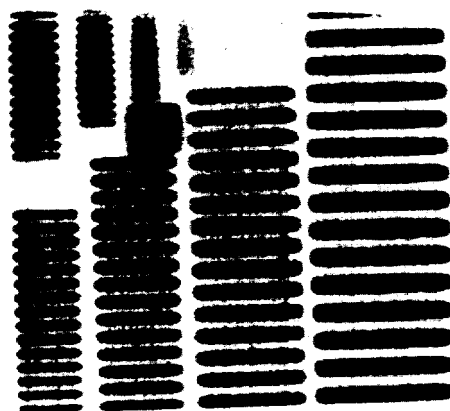




a. Coherence Interval  $2 \mu$   
(sodium source)



b. Coherence Interval  $25 \mu$



c. Incoherent Illumination

Figure 28. Photomicrographs  
of Square-Wave Target Under  
Various Conditions of Coher-  
ence (360X Magnification over  
original object)

## CHAPTER 6

SPECIAL CASES IN WHICH PARTIALLY COHERENT  
SYSTEM BECOMES LINEAR IN INTENSITY

## LOW-CONTRAST OBJECTS

As we saw in Chap. 2, a direct comparison cannot be made between incoherent and partially coherent imaging systems because of the nonlinearities involved. Such a comparison would be possible if the partially coherent system were completely characterized by an intensity impulse response or by its Fourier transform — the intensity modulation transfer function.

In this chapter we show that under certain conditions a partially coherent imaging system is linear in intensity when the objects used have constant phase and low contrast. (The question of how low the contrast must be will be examined at the end of the chapter.) An intensity modulation transfer function that completely characterizes a partially coherent imaging system and permits direct comparison with incoherent systems can then be defined. This type of approximation for low-contrast objects was first treated by Menzel<sup>7</sup> and later by Maréchal.<sup>8</sup>

For simplicity, we consider a one-dimensional system, unit magnification, and a single lens aperture. The object is in the  $\xi$  plane and the image in the  $x$  plane. The mutual intensity in the image plane is

$$\Gamma_i(x_1, x_2) = \iint \Gamma_o(\xi_1, \xi_2) t(\xi_1) t^*(\xi_2) K(x_1 - \xi_1) K^*(x_2 - \xi_2) d\xi_1 d\xi_2, \quad (92)$$

where  $\Gamma_o(\xi_1, \xi_2)$  is the mutual intensity of the radiation incident on the object,  $t(\xi)$  is the complex amplitude transmittance of the object (which we take to be of constant phase), and  $K(x - \xi)$  is the complex amplitude impulse response of the system.

Since Eq. (92) contains the product  $tt^*$ , the constant phase cancels. We may then take  $t$  to be real, i.e.,  $t = t^*$ . We represent a low-contrast object by

$$t(\xi) = t_o + t'(\xi), \quad (93)$$

where  $t_o$  is a constant and

$$t'(\xi) \ll t_o \quad (94)$$

Then we have

$$\begin{aligned} t(\xi_1) t^*(\xi_2) &= t(\xi_1) t(\xi_2) = [t_o + t'(\xi_1)] [t_o + t'(\xi_2)] \\ &\cong t_o^2 + t_o [t'(\xi_1) + t'(\xi_2)] \quad , \end{aligned} \quad (95)$$

where we have used Eq. (94) to obtain (95). We note for later reference that the intensity distribution in the object is, from (95),

$$I(\xi) = |t(\xi)|^2 \cong t_o^2 + 2t_o t'(\xi) \quad (96)$$

Using Eq. (95) in (92), we find

$$\begin{aligned} \Gamma_i(x_1, x_2) &= \iint \Gamma_o(\xi_1, \xi_2) \left\{ t_o^2 + t_o [t'(\xi_1) + t'(\xi_2)] \right\} \\ &\quad K(x_1 - \xi_1) K^*(x_2 - \xi_2) d\xi_1 d\xi_2 \quad . \end{aligned} \quad (97)$$

The intensity in the image plane is, from Eq. (97),

$$\begin{aligned} I_i(x) &= \Gamma_i(x, x) = t_o^2 \iint \Gamma_o(\xi_1, \xi_2) K(x - \xi_1) K^*(x - \xi_2) d\xi_1 d\xi_2 \\ &\quad + t_o \iint \Gamma_o(\xi_1, \xi_2) t'(\xi_1) K(x - \xi_1) K^*(x - \xi_2) d\xi_1 d\xi_2 \\ &\quad + t_o \iint \Gamma_o(\xi_1, \xi_2) t'(\xi_2) K(x - \xi_1) K^*(x - \xi_2) d\xi_1 d\xi_2 \quad , \end{aligned} \quad (98)$$

where we set  $x_1 = x_2 = x$ .

It is clear that the variables  $\xi_1$  and  $\xi_2$  are dummy variables in the integrations of (98), and so we may interchange  $\xi_1$  and  $\xi_2$  in the second term of (98) to obtain

$$\begin{aligned} I_1(x) = & t_o^2 \iint \Gamma_o(\xi_1, \xi_2) K(x - \xi_1) K^*(x - \xi_2) d\xi_1 d\xi_2 \\ & + t_o \int t'(\xi_2) \left\{ \int [\Gamma_o(\xi_2, \xi_1) K(x - \xi_2) K^*(x - \xi_1) \right. \\ & \left. + \Gamma_o(\xi_1, \xi_2) K(x - \xi_1) K^*(x - \xi_2)] d\xi_1 \right\} d\xi_2 . \end{aligned} \quad (99)$$

Now note that from Eq. (91) we have

$$\Gamma(\xi_2, \xi_1) = \Gamma^*(\xi_1, \xi_2) . \quad (100)$$

Clearly, when

$$K(x - \xi) = K^*(x - \xi) \quad (101)$$

and

$$\Gamma_o(\xi_1, \xi_2) = \Gamma_o^*(\xi_1, \xi_2) , \quad (102)$$

i.e., when both the amplitude impulse response and the mutual intensity of the object illumination are real, by using Eqs. (100), (101), and (102) in the second term of (99) we find that

$$\int \Gamma_o(\xi_2, \xi_1) K(x - \xi_2) K^*(x - \xi_1) d\xi_1 = \int \Gamma_o(\xi_1, \xi_2) K(x - \xi_1) K^*(x - \xi_2) d\xi_1 . \quad (103)$$

Then Eq. (99) becomes

$$I_1(x) = \int I_o(\xi_2) G(x, \xi_2) d\xi_2 , \quad (104)$$

where, from (96),

$$I_o(\xi_2) = t_o^2 + 2t_o t'(\xi_2) \quad (105)$$

is the intensity distribution in the object, and

$$G(x, \xi_2) = K(x - \xi_2) \int \Gamma_o(\xi_1, \xi_2) K(x - \xi_1) d\xi_1 \quad (106)$$

is the Green's function or intensity impulse response of the system.

Equation (104) represents a system linear in intensity. Examination of (99) shows that Eqs. (100) and (101) are sufficient conditions, rather than necessary ones, for (104). The necessary condition is actually (103).

Conditions (101) and (102) are realistic and are satisfied to a good approximation by the present system.

When the mutual intensity of the radiation incident on the object plane is spatially stationary, as it is for the laser and rotating ground glass illumination system, then we have

$$\Gamma_o(\xi_1, \xi_2) = \Gamma_o(\xi_1 - \xi_2) \quad (107)$$

and Eq. (106) becomes

$$G(x, \xi_2) = K(x - \xi_2) \int \Gamma_o(\xi_1 - \xi_2) K(x - \xi_1) d\xi_1 \quad (108)$$

Now make the change of variables

$$\xi = \xi_1 - \xi_2 \quad (109)$$

in Eq. (108) so that

$$\begin{aligned} G(x, \xi_2) &= K(x - \xi_2) \int \Gamma_o(\xi) K[(x - \xi_2) - \xi] d\xi \\ &= K(x - \xi_2) f(x - \xi_2) \end{aligned} \quad (110)$$

where

$$f(x - \xi_2) = \int_{-\infty}^{\infty} \Gamma_o(\xi) K[(x - \xi_2) - \xi] d\xi .$$

The conclusion from Eq. (110) is that

$$G(x, \xi_2) = G(x - \xi_2) \quad (111)$$

and therefore the intensity impulse response, or Green's function, of the system is spatially stationary.

The spatial frequency domain description of the system is then obtained by using Eq. (111) in (104) to obtain

$$I_i(x) = \int I_o(\xi_2) G(x - \xi_2) d\xi_2 , \quad (112)$$

and taking the spatial Fourier transform of Eq. (112), we then have

$$\tilde{I}_i(\nu) = \tilde{I}_o(\nu) T_{pc}(\nu) , \quad (113)$$

where  $T_{pc}(\nu)$  is the intensity modulation transfer function of the partially coherent imaging system. The quantities  $\tilde{I}_i(\nu)$  and  $\tilde{I}_o(\nu)$  are the Fourier transforms of the image and object intensity distributions respectively.

The definition of  $T_{pc}(\nu)$  is

$$T_{pc}(\nu) = \frac{\int_{-\infty}^{\infty} G(\xi) e^{2\pi i \xi \nu} d\xi}{\int_{-\infty}^{\infty} G(\xi) d\xi} , \quad (114)$$

where we have normalized so that  $T_{pc}(0) = 1$ .

We will now evaluate  $T_{pc}(\nu)$  for the elementary case of a rectangular incoherent slit source and a rectangular lens aperture. The source is in the  $\beta$  plane; the other planes are as in Eq. (92). The halfwidth of the rectangular source is  $b$  and that of the rectangular lens aperture is  $a$ . Magnification is unity. We assume that the size of the source is much less than its distance from the object plane.

The mutual intensity of the illumination incident on the object is, from the van Cittert-Zernike theorem (Eq. (99)),

$$\Gamma_o(\xi_1 - \xi_2) = \int_{-\infty}^{\infty} I(\gamma) e^{-2\pi i \gamma (\xi_1 - \xi_2)} d\gamma, \quad (115)$$

where

$$\gamma = \frac{\beta}{\lambda R}, \quad (116)$$

and the intensity distribution of the source is given by

$$I(\gamma) = \begin{cases} 1 & \left| \gamma \right| \leq \frac{b}{\lambda R} \\ 0 & \left| \gamma \right| > \frac{b}{\lambda R} \end{cases}. \quad (117)$$

A Fourier transform relation also holds between the lens aperture and the amplitude impulse response of the lens. Thus we have

$$K(\xi) = \int_{-\infty}^{\infty} A(\eta) e^{-2\pi i \eta \xi} d\eta, \quad (118)$$

where

$$\eta = \frac{\alpha}{\lambda S} \quad (119)$$

and the amplitude transmittance of the lens aperture is given by

$$A(\eta) = \begin{cases} 1 & |\eta| \leq \frac{a}{\lambda S} \\ 0 & |\eta| > \frac{a}{\lambda S} \end{cases} \quad (120)$$

Now using Eqs. (110) and (114), we find that  $T_{pc}(\nu)$  has the form

$$T_{pc}(\nu) = \frac{\int_{-\infty}^{\infty} K(\xi) \left[ \int_{-\infty}^{\infty} \Gamma_o(\xi') K(\xi - \xi') d\xi' \right] e^{2\pi i \xi \nu} d\xi}{\int_{-\infty}^{\infty} K(\xi) \left[ \int_{-\infty}^{\infty} \Gamma_o(\xi') K(\xi - \xi') d\xi' \right] d\xi} \quad (121)$$

Using the convolution theorem on the inner integrals in numerator and denominator of (121), we have

$$T_{pc}(\nu) = \frac{\int_{-\infty}^{\infty} K(\xi) \left[ \int_{-\infty}^{\infty} \tilde{\Gamma}_o(\nu') \tilde{K}(\nu') e^{-2\pi i \xi \nu'} d\nu' \right] e^{2\pi i \xi \nu} d\xi}{\int_{-\infty}^{\infty} K(\xi) \left[ \int_{-\infty}^{\infty} \tilde{\Gamma}_o(\nu') \tilde{K}(\nu') e^{-2\pi i \xi \nu'} d\nu' \right] d\xi} \quad (122)$$

$$= \frac{\int_{-\infty}^{\infty} \tilde{\Gamma}_o(\nu') \tilde{K}(\nu') \left[ \int_{-\infty}^{\infty} K(\xi) e^{2\pi i \xi (\nu - \nu')} d\xi \right] d\nu'}{\int_{-\infty}^{\infty} \tilde{\Gamma}_o(\nu') \tilde{K}(\nu') \left[ \int_{-\infty}^{\infty} K(\xi) e^{-2\pi i \xi \nu'} d\xi \right] d\nu'} \quad (123)$$

$$= \frac{\int_{-\infty}^{\infty} \tilde{\Gamma}_o(\nu') \tilde{K}(\nu') \tilde{K}(\nu - \nu') d\nu'}{\int_{-\infty}^{\infty} \tilde{\Gamma}_o(\nu') \tilde{K}(\nu') K(-\nu') d\nu'} \quad (124)$$



We can evaluate (124) with Eqs. (115) through (120). The variables  $a/\lambda S$  and  $b/\lambda R$  are the usual diffraction variables that arise in problems of this type. We will therefore redefine them to be

$$a' = \frac{a}{\lambda S} \quad \text{and} \quad b' = \frac{b}{\lambda R} .$$

The evaluated form of  $T_{pc}(\nu)$  is then, for  $\nu \geq 0$ ,

$$T_{pc}(\nu) = \begin{cases} 0 & \nu > 2a' \text{ or } \nu > a' + b' \\ 1 & a' > b' \text{ and } 0 \leq \nu \leq a' - b' \\ 1 - \frac{\nu}{a' + b'} & a' > b' \text{ and } a' - b' < \nu \leq a' + b' \\ 1 - \frac{\nu}{2a'} & a' \leq b' \text{ and } 0 \leq \nu \leq 2a' \end{cases} \quad (125)$$

Using (114) and (110) we can easily show that, by a change of variables,

$$T_{pc}(\nu) = T_{pc}(-\nu) . \quad (126)$$

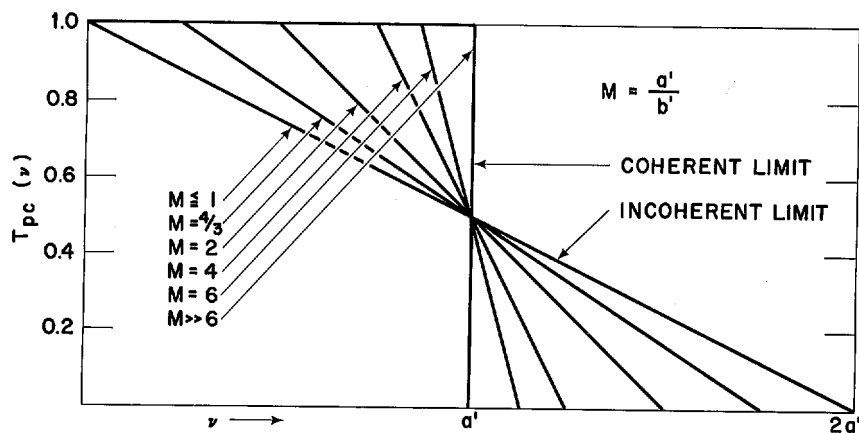
Then (125) and (126) define  $T_{pc}(\nu)$ . It is clear that  $T_{pc}(\nu)$  is real, i.e.,

$$T_{pc}(\nu) = T_{pc}^*(\nu) . \quad (127)$$

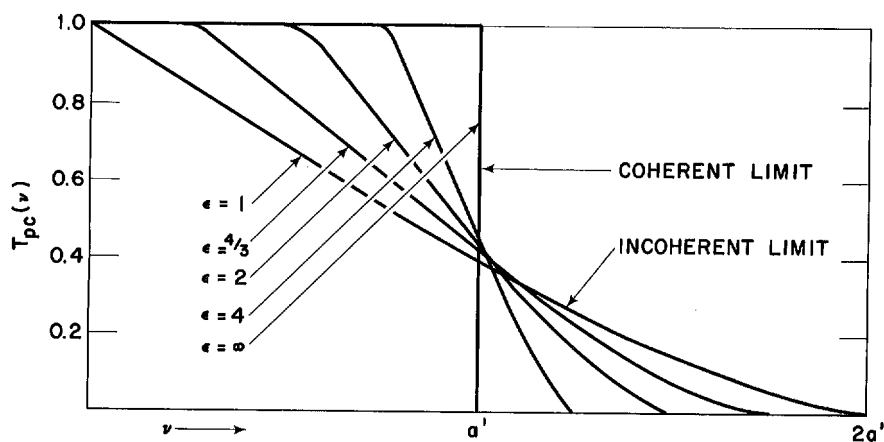
Figure 29a shows Eq. (125) for various ratios  $M$  of  $a'$  to  $b'$ . A similar calculation for the case of a circular source and circular lens aperture is also shown in Figure 29b for various ratios  $\epsilon$  of the radius of the lens to the radius of the source.

### OBJECTS WITH LOW SPATIAL-FREQUENCY CONTENT

Another case in which the partially coherent imaging system is completely characterized by an intensity impulse response or its Fourier transform — the intensity modulation transfer function — is that of objects having low spatial-frequency content. Figure 30 is an example of such an object; here the object structure  $t(\xi)$

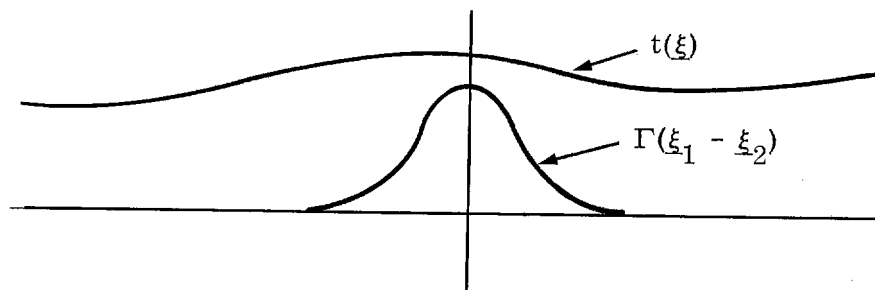


a. Cylindrical Lens



b. Spherical Lens

Figure 29. Transfer Functions for Ideal Lens Imaging Low-Contrast Objects with Partially Coherent Illumination

Figure 30. Slowly Varying Object  $t(\xi)$  vs Mutual Intensity Function  $\Gamma(\xi_1 - \xi_2)$

varies slowly over distances in which the mutual intensity function  $\Gamma(\xi_1 - \xi_2)$  is non-zero.

Using the general imaging equation ((18) in Chap. 2),

$$I(\underline{x}) = \iint \Gamma(\xi_1 - \xi_2) t(\xi_1) t^*(\xi_2) K(\underline{x} - \xi_1) K^*(\underline{x} - \xi_2) d\xi_1 d\xi_2, \quad (128)$$

and letting  $\xi_1 - \xi_2 = \underline{\sigma}$ , we have

$$I(\underline{x}) = \iint \Gamma(\underline{\sigma}) t(\xi_2 + \underline{\sigma}) t^*(\xi_2) K(\underline{x} - \underline{\sigma} - \xi_2) K^*(\underline{x} - \xi_2) d\xi_2 d\underline{\sigma}. \quad (129)$$

Now when the changes in  $t(\xi_2 + \underline{\sigma})$  are small in the distance  $\underline{\sigma}$  over which  $\Gamma(\underline{\sigma})$  is non-zero, we may make the approximation that

$$t(\xi_2 + \underline{\sigma}) \cong t(\xi_2). \quad (130)$$

If we then use (130), Eq. (129) becomes

$$I(\underline{x}) = \int t(\xi_2) t^*(\xi_2) \left\{ K^*(\underline{x} - \xi_2) \int \Gamma(\underline{\sigma}) K[(\underline{x} - \xi_2) - \underline{\sigma}] d\underline{\sigma} \right\} d\xi_2. \quad (131)$$

Therefore, we have

$$I(\underline{x}) = \int I(\xi_2) G(\underline{x} - \xi_2) d\xi_2, \quad (132)$$

which is a linear intensity superposition integral in which

$$G(\underline{x} - \xi_2) = K^*(\underline{x} - \xi_2) \int \Gamma(\underline{\sigma}) K[(\underline{x} - \xi_2) - \underline{\sigma}] d\underline{\sigma} \quad (133)$$

is the intensity impulse response of the system.

Interestingly enough, Eq. (133) has the same form as (110) when  $K(\underline{x} - \underline{\xi})$  is real. For this case, then, the transfer functions shown in Figure 29 will apply to Eq. (132).



The question then arises: Will transparencies that satisfy the criterion of low contrast or of low spatial-frequency content actually occur in practice?

Low spatial-frequency content is readily interpretable mathematically, but it otherwise presents problems. The first difficulty is that this requirement is in terms of the amplitude transmittance of the transparency, and this quantity cannot be readily determined for general scenes. The more important consideration is that if the spatial frequency content of the scene is low, then incoherent illumination can be used in the imaging process without significant loss of detail.

The low-contrast approximation is also difficult to interpret. A measure of how low the contrast must be could not be determined. Further experimental work would be necessary to properly assess the applicability of these two approximations to practical enlarging applications.

## CHAPTER 7

## PARTICULAR COHERENCE EFFECTS

## COHERENCE NOISE

In an ideal imaging system, the light arriving at a point in the image plane will have originated at a small area around the corresponding point in the object plane. The size of this area is dependent on the spread function of the lens. In practice, however, some light reaching an image point will arise from other areas because of scattering by foreign particles in the system and multiple reflections from lens elements. In incoherent imagery, where all light adds in intensity, this will result in a reduction in image contrast. In coherent imagery, this light can interfere with the true image light and with other stray light, resulting in a noisy image.

There are three possible ways to lessen this noise:

1. The optical system can be made as clean as possible and the antireflection coatings on the lenses as efficient as possible to minimize stray light. Even the best lenses available, however, exhibit a considerable amount of coherence noise.
2. The coherence interval can be made as small as possible consistent with other requirements. This minimizes the area in the object plane from which light reaching a point in the image plane can interfere.
3. The coherence length can be made as small as possible consistent with other requirements. This places a limit on the path difference that two rays reaching a point in the image plane can have undergone and still interfere.

Figure 31 illustrates the reduction in noise using the laser-illuminated rotating ground glass system as the coherence interval in the object plane is decreased. For the longer coherence intervals, the noise consists of several recognizable diffraction patterns from dirt particles, with a general mottling over the entire field. The mottling decreases as the coherence interval decreases; the diffraction patterns remain, although the extent of the patterns decreases.

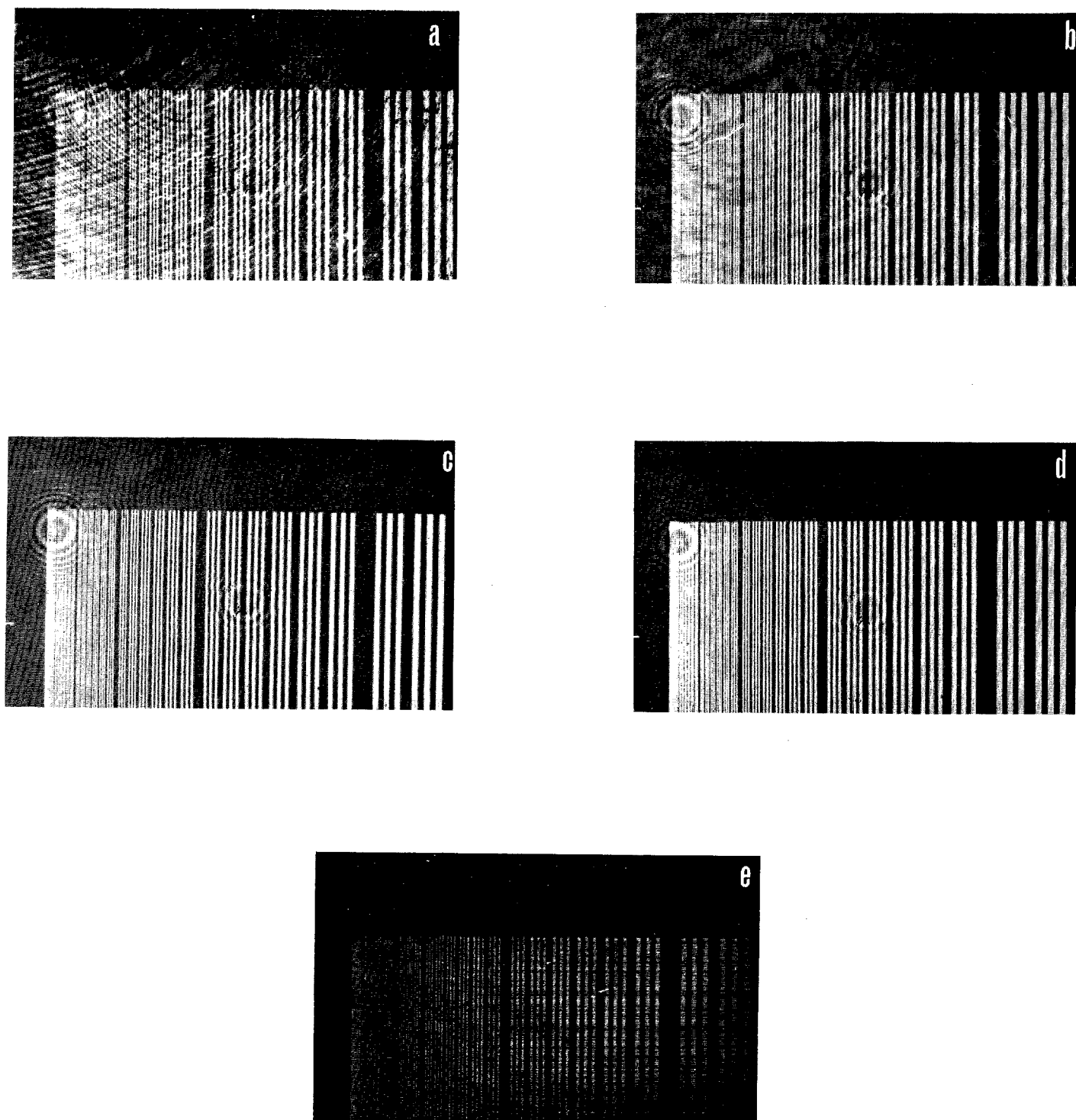


Figure 31. Example of Coherence Noise: Images of Low-Contrast "L" Targets for Coherent Illumination (a); for Coherence Intervals of 8 mm (b), 230  $\mu$  (c), and 80  $\mu$  (d); and for Incoherent Illumination (e)

The same qualitative effects would be observed if the coherence interval remained large but the coherence length was decreased. (The coherence length of the laser is considerably greater than is required to satisfy the quasi-monochromatic approximation.)

### EXAMPLE OF NONLINEAR EFFECTS

In Chap. 2 we showed that a partially coherent imaging system is, in general, nonlinear in intensity and therefore cannot be characterized by a modulation transfer function (see Chap. 6 for special cases in which a partially coherent system becomes linear in intensity).

To illustrate the meaning of this statement graphically, we present below an example of the application of linear systems analysis in a case where it should not be applied — to the present nonlinear enlarger system. The technique was as follows. A theoretical apparent transfer function, such as those described in Chap. 2 and calculated for the edge images in Chap. 5, was found for an edge object at  $D = 16$  (this quantity is defined in Chap. 5). If the system were linear in intensity, then Eq. (14a) would apply and the apparent transfer function should be a valid transfer function. It should then be possible to calculate the Fourier transform of the image intensity distribution for any object by multiplying the Fourier transform of the object intensity distribution by this transfer function determined from the edge object. Taking the inverse Fourier transform would then yield the image intensity distribution.

In our work we took as objects particular three-bar groups in the  "L" target. The first object was the 203  $\ell$ /mm group in a 2:1 contrast target. The second was the 256  $\ell$ /mm group in an effectively infinite-contrast target. These objects are shown as the B curves in Figures 32 and 33. The adjacent three-bar groups are not shown in the figures but were included in calculations as a first approximation to the effects of interaction between groups.

The calculated images shown as the A curves in Figures 32 and 33 were then found using the general partially coherent imaging equation ((18) in Chap. 2) and the program described in Appendix B. We assumed a 225  $\ell$ /mm coherent cutoff frequency.

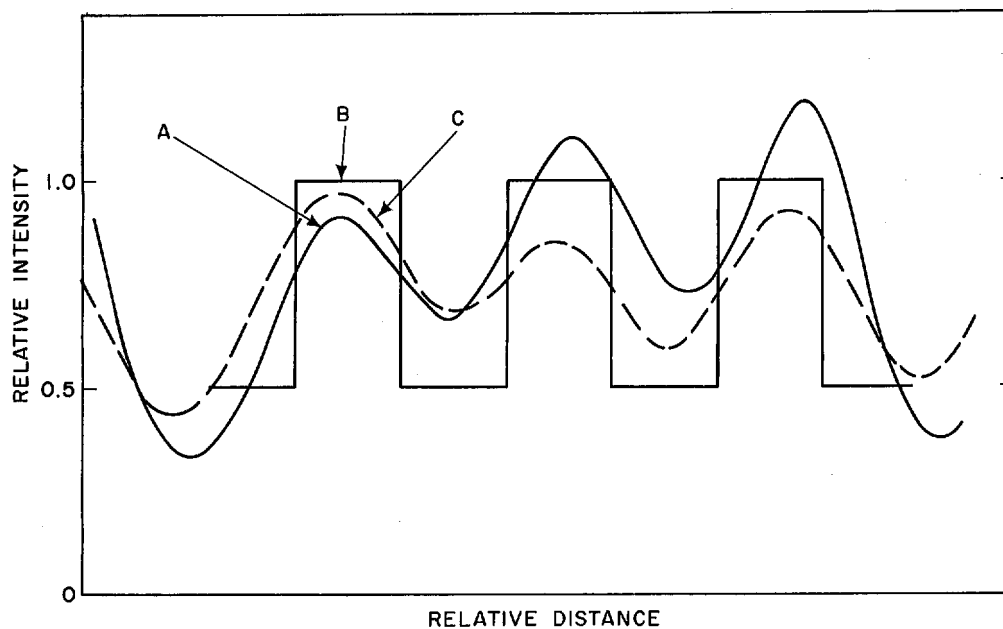


Figure 32. Calculated Image A of 2:1-Contrast 203  $\ell/\text{mm}$  Three-Bar Group B and Image C Calculated from Apparent Edge Transfer Function for  $D = 1/16$  and Coherent Cutoff Frequency of 225  $\ell/\text{mm}$

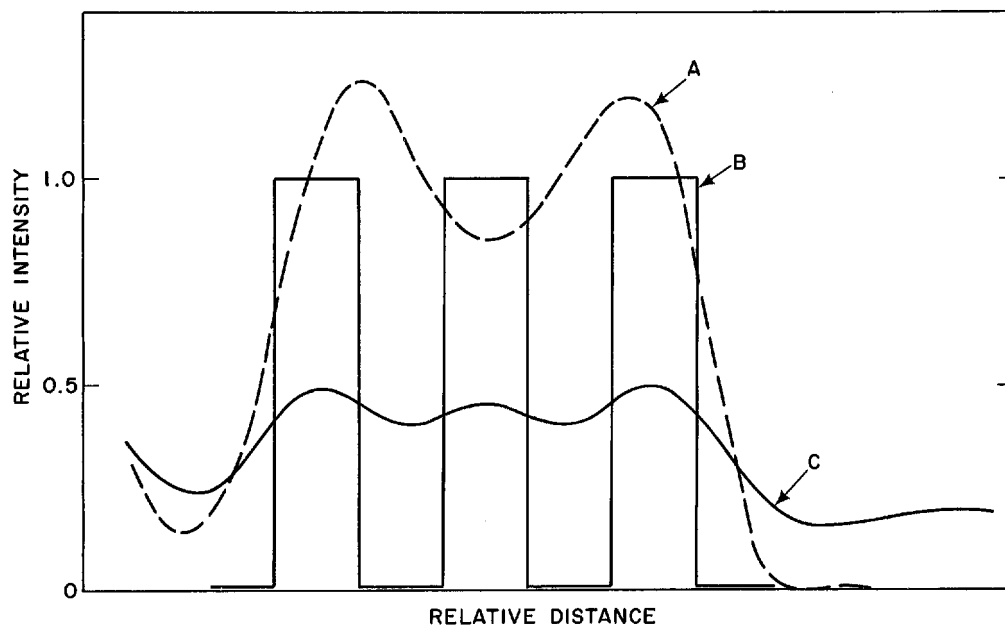


Figure 33. Calculated Image A of Infinite-Contrast 256  $\ell/\text{mm}$  Three-Bar Group B and Image C Calculated from Apparent Edge Transfer Function for  $D = 1/16$  and Coherent Cutoff Frequency of 225  $\ell/\text{mm}$



Next, to find an image intensity distribution, the apparent transfer function described above was used as if the system were linear. These images are shown as the C curves in Figures 32 and 33.

It is obvious from Figure 32 that the images calculated by the two techniques described — one valid (A) and the other invalid (C) — are qualitatively the same although quantitatively different. Both show the three-bar object producing a three-bar image. However, Figure 33 shows that the theoretical image of this three-bar group looks like two bars, whereas the invalid image calculated from the apparent transfer function still appears as three bars.

Thus the nonlinear effects in partially coherent imaging are considerable, and the fact that they are not pronounced in one case (Figure 32) does not mean that they will not be in another (Figure 33).



## CHAPTER 8

## SPATIAL FILTERING APPLICATIONS

When a transparency in the front focal plane of a lens is illuminated by a spatially coherent, quasi-monochromatic beam of light, the two-dimensional Fourier transform of the amplitude transmittance appears in the back focal plane and it can then be retransformed by a second lens to give an image of the original object. This is essentially the situation that exists in the present enlarger when it is used with a high degree of spatial coherence. By placing various filters in the back focal plane (transform plane) of the first lens, the amplitude frequency spectrum, and thus the resultant image, can be altered. Such a procedure may be used to remove unwanted information from a scene or to enhance information about certain frequencies over that of other frequencies.

## RASTER REMOVAL

Let the amplitude transmittance of the object transparency be represented by  $f(x, y)$ , where  $x$  and  $y$  are the coordinates in the object plane. Then the Fourier transform, which will appear in the transform plane, is given by

$$F(\gamma, \mu) = \int_{-\infty}^{\infty} \int_{-\infty}^{\infty} f(x, y) e^{2\pi i(\gamma x + \mu y)} dx dy, \quad (134)$$

where  $\gamma$  and  $\mu$  are spatial frequency coordinates related to the spatial coordinates  $\eta$  and  $\xi$  by

$$\gamma = \frac{\eta}{\lambda f} \quad \mu = \frac{\xi}{\lambda f}.$$

Upon retransformation, the amplitude distribution in the image plane becomes

$$f'(x', y') = \iint F(\gamma, \mu) e^{2\pi i(\gamma x' + \mu y')} d\gamma d\mu. \quad (135)$$

For a transparency of a scene containing linear raster lines parallel to the x axis, the amplitude distribution can be written

$$f(x, y) = s(x, y) r(y) , \quad (136)$$

where  $s(x, y)$  describes the scene and  $r(y)$  describes the raster. If we assume that  $r(y)$  is an infinite square wave, then  $r(y)$  can be represented by a Fourier series:

$$r(y) = 1 + \frac{4}{\pi} \sum_{n=0}^{\infty} \frac{1}{n+1} \frac{\sin (n+1) 2\pi y}{p} \quad n = 0, 1, 2 \quad (137)$$

where  $p$  is the period of the square wave.

The function

$$\begin{aligned} F(\gamma, \mu) &= \iint s(x, y) r(y) e^{2\pi i(\gamma x + \mu y)} dx dy \\ &= \iint s(x, y) e^{2\pi i(\gamma x + \mu y)} dx dy \\ &\quad + \frac{4}{\pi} \sum_{n=0}^{\infty} \iint s(x, y) \frac{1}{n+1} \frac{\sin (n+1) 2\pi y}{p} e^{2\pi i(\gamma x + \mu y)} dx dy \end{aligned} \quad (138)$$

will appear in the transform plane. The first term in (138) is the one that would appear in the transform plane if there were no raster on the original scene. If all the other terms can be removed, retransformation will yield the desired scene image with no raster.

Each term in the infinite series is the Fourier transform of the product of two functions. This is equal to the convolution of the Fourier transforms of the functions. Let the infinite series be represented by  $F'(\gamma, \mu)$ ; we then have

$$F'(\gamma, \mu) = \frac{4}{\pi} \sum_{n=0}^{\infty} \int_{-\infty}^{\infty} \int_{-\infty}^{\infty} s(\gamma', \mu') R_n(\gamma - \gamma', \mu - \mu') d\gamma' d\mu' \quad (139)$$

$$R_n(\gamma', \mu') = \frac{1}{n+1} \int_{-\infty}^{\infty} \int_{-\infty}^{\infty} \frac{\sin 2\pi(n+1)y}{p} e^{2\pi i(\gamma'x + \mu'y)} dx dy \quad (140)$$

Performance of the integration yields

$$R_n(\gamma', \mu') = \frac{\delta(\gamma')}{2i(n+1)} \left\{ \delta \left[ \left( \frac{n+1}{p} \right) + \mu' \right] - \delta \left[ \left( \frac{n+1}{p} \right) - \mu' \right] \right\} \quad (141)$$

We now have

$$\begin{aligned} F'(\gamma', \mu) &= \frac{2}{\pi i} \sum_{n=0}^{\infty} \frac{1}{n+1} \int_{-\infty}^{\infty} \int_{-\infty}^{\infty} s(\gamma', \mu') \left\{ \left[ \delta(\gamma' - \gamma) \right] \delta \left[ \left( \frac{n+1}{p} \right) + \mu - \mu' \right] \right. \\ &\quad \left. - \delta \left[ \left( \frac{n+1}{p} \right) - \mu + \mu' \right] \right\} d\gamma' d\mu' \quad (142) \\ &= \frac{2}{\pi i} \sum_{n=0}^{\infty} \frac{1}{(n+1)} \left[ s \left( \gamma, \frac{n+1}{p} + \mu \right) - s \left( \gamma, \frac{n+1}{p} - \mu \right) \right] . \end{aligned}$$

Each term in the series is the Fourier transform of  $s(x, y)$  with a different position along the  $\mu$  axis. The terms are spaced a distance of  $\lambda f/p$  apart along the  $\xi$  axis on both sides of the optical axis. The required filter is thus an opaque strip along the  $\xi$  axis having a transparent region of width approximately  $\lambda f/p$  centered on the axis.

In general, the raster function will not be a perfect square wave, but will be some periodic function representable by a Fourier series. For each period  $p$  in this series, there will be transforms of  $s(x, y)$  along the  $\xi$  axis at distances of  $\pm \lambda f/p$  from the axis.

Figure 34 is an example of raster removal on transparencies produced by direct electron beam recording of commercial television scenes. The fundamental raster frequency was 10  $\ell/\text{mm}$ . For the 9 in. lens,  $\lambda f/p = 1.45$  mm was used. The filter consisted of a bar 2 mm in height with a central opening of 1.4 mm. It is evident in the photographs that when the coherence interval was in excess of 1 mm, raster removal was quite effective — only a slight low-frequency modulation remained. At the coherence interval of 25  $\mu$ , many of the objectionable artifacts disappeared, but the raster removal was far less efficient. In this case, the coherence interval did not extend over a raster period, so efficient removal was not expected. A more effective system would use light of a shorter coherence length so that the stray artifacts would be reduced even for large coherence intervals. With the sodium source, however, the required coherence interval could not be obtained at reasonable intensity levels.

Another example of raster removal using the techniques discussed in this chapter is included in Appendix C.

#### FILTERS SUPPLIED WITH ENLARGER

The transfer function of the camera with which a negative is made will generally be a decreasing function of spatial frequency. Spatial filtering offers an opportunity to somewhat reverse this effect by suppressing the lower frequencies relative to the higher ones. A filter to accomplish this would have decreasing density away from the center of the transform plane. Again, however, this is a nonlinear imaging process requiring both the amplitude distribution across the object and the amplitude transmittance of the filter for a complete understanding.

Seven filters with approximately a Gaussian intensity taper were supplied by Perkin-Elmer with the enlarger. All had a peak density of about 1, and varied in half-intensity width from 0.2 cm to 1.1 cm, which corresponded to about 4  $\ell/\text{mm}$

25X1

Approved For Release 2002/07/12 : CIA-RDP78B04747A002700020022-7


Approved For Release 2002/07/12 : CIA-RDP78B04747A002700020022-7

to 20  $\ell$ /mm in frequency in the transform. Since the frequency range covered by the broader filters seemed fairly compatible with the aerial scenes described in Chap. 5, tests were conducted to see if these filters had any effect on these negatives. The entire range of filters was used, but the only effect observed was some mottling in the fine structure of the filtered images. No noticeable enhancement of the high-frequency information in the scenes occurred. However, since the amplitude distributions of neither the aerial scenes nor the filters are known, it is not possible to specify what effects would be expected theoretically.



## CHAPTER 9

## CONCLUSIONS AND RECOMMENDATIONS

25X1  Coherent Enlarger has been evaluated and the following conclusions have been reached:

1. Direct experimental measurement of the coherence of the object plane illumination, when the light source is the rotating ground glass disc illuminated by the single mode laser, shows that the illuminated rotating ground glass disc acts as an incoherent source. The coherence of the object plane illumination is simply that predicted by the well known van Cittert-Zernike theorem. Specifically, we found that the intensity distribution in the plane of the ground glass was Gaussian. The predicted mutual intensity (coherence) distribution in the object plane is then also a Gaussian whose width is determined by the Fourier transform relation between these two Gaussian functions. The measured mutual intensity (coherence) function in the object plane was in excellent agreement with this prediction. The coherence was found, as predicted from the van Cittert-Zernike theorem, to be a function only of the distance between the two measurement points and not of the location of the individual points. Theoretical predictions of the expected coherence in the object plane when the multimode laser illuminated the ground glass were not made because of the complexity of the multimode laser intensity pattern. However, experimental measurements indicated that the illuminated rotating ground glass disc acted as an incoherent source in this case also.

2. The on-axis incoherent modulation transfer function of the enlarger was shown to be very close to the transfer function of a diffraction-limited optical system. This transfer function was determined by microdensitometer and computer analyses of experimental edge images. Images of USAF three-bar targets illuminated with incoherent light showed that the on-axis resolution is maintained over an approximately 1.5 in. diameter-object format. The theoretical and experimental sections of this report show that when the object is illuminated by coherent or partially coherent light, the instrument's performance cannot generally be described by the customary image evaluation criteria and techniques such as a transfer function or a resolution value. The general partially coherent imaging theory must be used to predict the effect of the system on each object individually.



3. Images calculated from the general partially coherent imaging equation agree well with the measured images. It is therefore concluded that the theory of partial coherence, as presented in the theoretical sections of this report, provides a satisfactory description of the imaging properties of this enlarger.

4. It was determined experimentally that when an object contains only spatial frequencies much lower than the coherent cutoff frequency of the enlarger, there is little if any noticeable difference between the images of this object obtained using coherent, partially coherent, or incoherent illumination. However when there is considerable spatial frequency content at or near the coherent cutoff frequency of the enlarger, the effects of the coherence of the illumination are pronounced: images can appear completely changed in structure (a group of three bars becoming two bars, for example), the positions of edges shift, and structure appears in portions of the scene in which the object did not contain structure.

5. As an incoherent enlarger, the instrument is superior to existing commercial enlargers. Commercial enlarger lenses are generally well corrected at  $f/5.6$  or  $f/8$ , whereas the imaging system in this enlarger is well corrected at  $f/3.5$ . Routine use of this instrument as an incoherent enlarger requires minor mechanical modification.

6. Raster removal and other spatial filtering operations can be done conveniently with minor mechanical modification of the filter plane aperture. The earlier conclusions on partially coherent imaging apply to this filtering operation however.

7. Making images in partially coherent and incoherent illumination of aerial scene transparencies in which the resolution limit is at or beyond the coherent cutoff frequency of the enlarger system would be informative. A determination should be made of the effects of coherence on the interpretation of these images.

8. It should be pointed out that for those cases where maximum correspondence between object and image is required, the enlarger should be used in its incoherent mode, i.e., as a linear imaging system. Until such time as high quality negatives are available for evaluation with the enlarger we can not definitely state the advantages to be gained by using the enlarger coherently, since the extent of image distortions introduced by the field coherence will vary with the target and the degree of coherence.



## REFERENCES

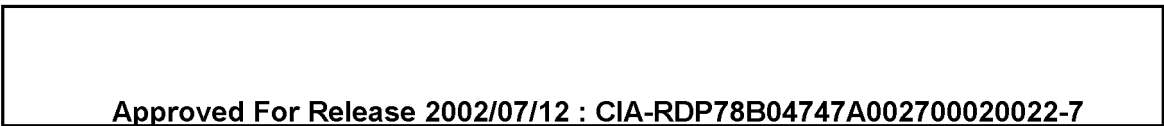
1. E. Wolf, Proc. Roy Soc. (A) 230, 246 (1954).
2. M. Born and E. Wolf, "Principles of Optics," 2nd ed. (New York, N.Y.: Pergamon Press, 1964).
3. M. Beran and G.B. Parrent, "Theory of Partial Coherence" (Englewood Cliffs, N.J.: Prentice-Hall, Inc., 1963).
4. T. Skinner, "Energy Considerations, Propagation in a Random Medium and Imaging in Scalar Coherence Theory" (Ph.D. Thesis, Boston University, 1964).
5. E.L. O'Neill, "Introduction to Statistical Optics" (Reading, Mass.: Addison-Wesley Publishing Co., 1962), p. 99.
6. B.J. Thompson and E. Wolf, J. Op. Soc. Am. 47, 895-902 (1957).
7. E. Menzel, Optik 15, 460-470 (1958).
8. A. Maréchal and M. Françon, "Diffraction Structures des Images" (Paris: Editions de la Revue d'Optique Theorique et Instrumental, 1960), Tome 2.

25X1

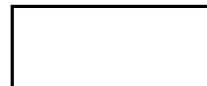


Approved For Release 2002/07/12 : CIA-RDP78B04747A002700020022-7

25X1



Approved For Release 2002/07/12 : CIA-RDP78B04747A002700020022-7



## A P P E N D I X E S

- A. AERIAL SCENES
- B. COMPUTER PROGRAM FOR FINDING THE  
INTENSITY IN THE IMAGE OF A PARTIALLY  
COHERENT OBJECT
- C. RASTER REMOVAL

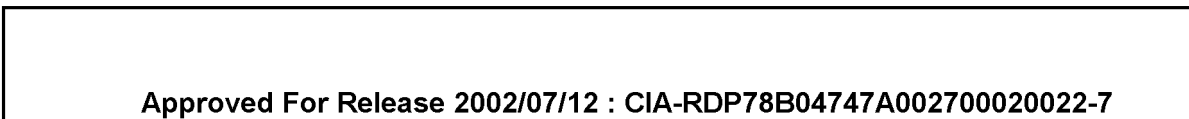
25X1

Approved For Release 2002/07/12 : CIA-RDP78B04747A002700020022-7



25X1

Approved For Release 2002/07/12 : CIA-RDP78B04747A002700020022-7



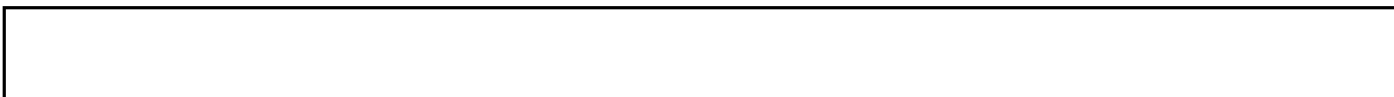
**CONFIDENTIAL**

## APPENDIX A

## AERIAL SCENES

Unfortunately, no photographs of aerial scenes containing information near the spatial frequency limits of this instrument were available for testing. Such photographs would indicate how severe a problem the various coherence effects might be for a photointerpreter. Some aerial scenes were imaged, however, and their spatial frequency content was determined by tracing a number of edges in the scenes with a microdensitometer and analyzing the frequency content of the sharpest edge. The frequency cutoff of the sharpest edges was about 60  $\ell$ /mm.

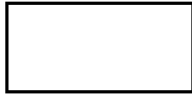
The only noticeable difference between the images of a given scene made with coherent and incoherent illumination was a higher noise content (see discussion of coherence noise in Chap. 7) in the images made with coherent light. This noise was primarily diffraction patterns from dust particles. Figures A-1 and A-2 are examples of these images. The image in Figure A-1 was made with coherent light; that in Figure A-2 with incoherent light.

**CONFIDENTIAL**

25X1

Approved For Release 2002/07/12 : CIA-RDP78B04747A002700020022-7

Approved For Release 2002/07/12 : CIA-RDP78B04747A002700020022-7



## APPENDIX B

COMPUTER PROGRAM FOR FINDING  
THE INTENSITY IN THE IMAGE  
OF A PARTIALLY COHERENT OBJECT

The basic integral for finding the intensity in the image of a partially coherently illuminated object is

$$I(y) = \int_{-\infty}^{\infty} \int_{-\infty}^{\infty} \Gamma(x_1, x_2) t(x_1) t^*(x_2) U(y - x_1) U^*(y - x_2) dx_1 dx_2$$

$t(x)$  = amplitude transmittance of the object

$\Gamma(x_1, x_2)$  = mutual intensity in the object plane as a function of the points  $x_1$  and  $x_2$

$U(x)$  = amplitude impulse response of the imaging lens.

This is essentially the integral that has been programmed in FORTRAN IV (Ver. 13) for the IBM 7094-II system.

Other forms of calculating  $I(y)$  were investigated, but since they offered no saving of time or computer instructions, they were abandoned in favor of this direct approach. Writing the above integral in summation form

$$I(y_m) = \sum_{j=1}^N \sum_{k=1}^N \Gamma_{jk} t_j t_k^* U_{mj} U_{mk}^* \Delta x_j \Delta x_k$$

and noting that the quantities  $\Gamma$ ,  $t$ , and  $U$  are generally complex, we may observe that any calculation of  $I(y_m)$  necessitates the calculation and storage of  $2N^2$  values of the integrand for minimum computer calculating time. Hence, a 100 point input requires 20,000 storage locations in the computer, which nearly reaches the limit of available space in the 7094. When it was ascertained that more than 100 data points were required to do the simple calculation of edge imaging, considerable



effort was spent in rewriting the program to handle the input data and intermediate calculations in blocks. By this method the program can handle up to 200 data points, calculating up to 80,000 values of the integrand in the most general case. However, since this method would be a considerable waste of computer time for some simple problems, legs were added to the program, where possible, to shorten calculating time. For instance there is a leg to handle the special case in which the mutual intensity and lens impulse response are functions of coordinate separation and, as a special case of that, the case where they are of the form  $\sin k(x_1 - x_2)/k(x_1 - x_2)$ . The block diagram in Figure B-1 gives additional details on this program.

The body of the FORTRAN IV (Ver. 13) computer program written under this contract follows. It should be noted that the program was written for a broad class of problems. During the course of this contract, occasion did not arise for testing out and using all segments of the program. In particular, the option to calculate the mutual intensity (gamma) as the output of an imaging system with an incoherent source was not used or tested. There is, therefore, no guarantee that this portion is devoid of errors.

25X1

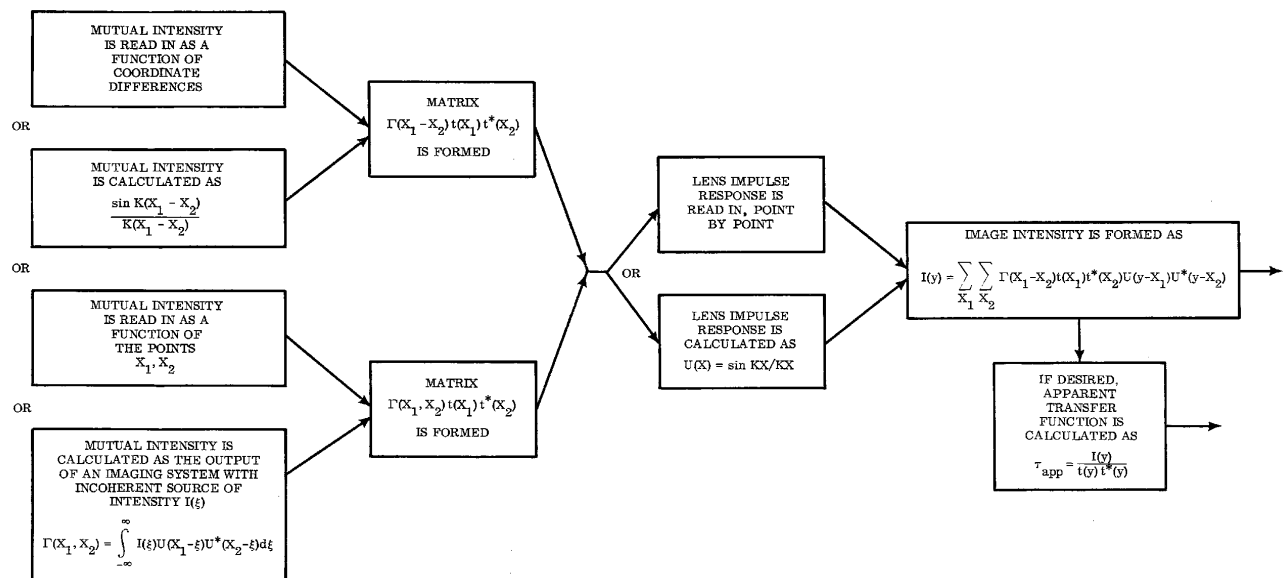


Figure B-1. Block Diagram of Computer Program

25X1

25X1

Approved For Release 2002/07/12 : CIA-RDP78B04747A002700020022-7

Next 4 Page(s) In Document Exempt

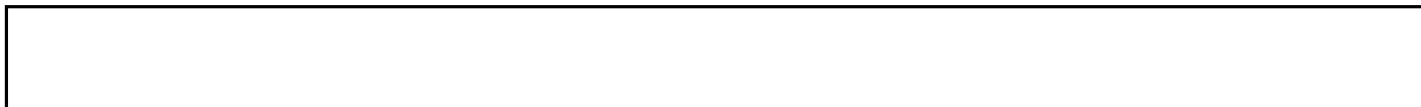
Approved For Release 2002/07/12 : CIA-RDP78B04747A002700020022-7

**CONFIDENTIAL**

## APPENDIX C

### RASTER REMOVAL

Figure C-1 is an example of raster removal from an aerial scene using the techniques discussed in Chap. 8. Although the raster is linear, it contains more than one basic frequency. The 1 mm bar separation is noticeably more efficient in removing the raster than the 2 mm separation, but it also filters out a considerable amount of the scene information.

**CONFIDENTIAL**

25X1

Approved For Release 2002/07/12 : CIA-RDP78B04747A002700020022-7

Next 1 Page(s) In Document Exempt

Approved For Release 2002/07/12 : CIA-RDP78B04747A002700020022-7